

1 **A connectome of a learning and memory center in the adult *Drosophila* brain**

2

3

4 Shin-ya Takemura*, Yoshinori Aso, Toshihide Hige, Allan Wong, Zhiyuan Lu, C. Shan
5 Xu, Patricia K. Rivlin, Harald Hess, Ting Zhao, Toufiq Parag, Stuart Berg, Gary Huang,
6 William Katz, Donald J. Olbris, Stephen Plaza, Lowell Umayam, Roxanne Aniceto, Lei-
7 Ann Chang, Shirley Lauchie, Omotara Ogundeyi, Christopher Ordish, Aya Shinomiya,
8 Christopher Sigmund, Satoko Takemura, Julie Tran, Glenn C. Turner, Gerald M.
9 Rubin and Louis K. Scheffer*

10

11

12 Janelia Research Campus, HHMI, Ashburn, VA, USA

13

14

15 *Corresponding authors:

16 takemuras@janelia.hhmi.org; Phone 571-209-4286

17 schefferl@janelia.hhmi.org; Phone 571-209-4151

18

19

20

21

22 **Abstract**

23

24 Understanding memory formation, storage and retrieval requires knowledge of the
25 underlying neuronal circuits. In *Drosophila*, the mushroom body (MB) is the major
26 site of associative learning. We reconstructed the morphologies and synaptic
27 connections of all 983 neurons within the three functional units, or compartments,
28 that compose the adult MB's α lobe, using a dataset of isotropic 8-nm voxels
29 collected by focused ion-beam milling scanning electron microscopy. We found that
30 Kenyon cells (KCs), whose sparse activity encodes sensory information, each make
31 multiple *en passant* synapses to MB output neurons (MBONs) in each compartment.
32 Some MBONs have inputs from all KCs, while others differentially sample sensory
33 modalities. Only six percent of KC>MBON synapses receive a direct synapse from a
34 dopaminergic neuron (DAN). We identified two unanticipated classes of synapses,
35 KC>DAN and DAN>MBON. DAN activation produces a slow depolarization of the
36 MBON in these DAN>MBON synapses and can weaken memory recall.

37

38 **Introduction**
39
40 Associative memory helps animals adapt their behaviors to a dynamically changing
41 world. The molecular mechanisms of memory formation are thought to involve
42 persistent changes in the efficiency of synaptic transmission between neurons. In
43 associative learning, persistent changes in synaptic efficacy correlated with memory
44 formation have been found at points of convergence between two neuronal
45 representations: one providing information from sensory inputs about the outside
46 world and a second indicating whether the current environment is punitive or
47 rewarding. Such sites of convergence have been identified for multiple forms of
48 associative learning (Medina et al., 2002, Ardiel and Rankin, 2010, Tovote et al.,
49 2015, Kandel and Schwartz, 1982). However, a comprehensive synaptic level
50 description of connectivity at such a site of convergence is not available for an
51 animal as complex as the fruit fly, *Drosophila*.
52
53 The mushroom body (MB) is the center of associative learning in insects (Erber et
54 al., 1980, Heisenberg et al., 1985, de Belle and Heisenberg, 1994, Dubnau et al.,
55 2001, McGuire et al., 2001, Mizunami et al., 1998). Sensory information enters the
56 MB via the calyx, where the dendritic claws of Kenyon cells (KCs) receive synaptic
57 inputs from projection neurons of olfactory and other modalities including visual,
58 gustatory and thermal (Vogt et al., 2016, Kirkhart and Scott, 2015, Yagi et al., 2016,
59 Caron et al., 2013, Stocker et al., 1990, Wong et al., 2002, Strausfeld, 1976, Tanaka et
60 al., 2004, Liu et al., 2015, Frank et al., 2015). The parallel axonal fibers of the KCs
61 form the MB-lobes, the output region of the MB. A pattern of sparse activity in the
62 KC population represents the identity of the stimulus. This sparseness is
63 maintained through two mechanisms. First, individual KCs generally only spike
64 when they receive simultaneous inputs from multiple projection neurons
65 (Gruntman and Turner, 2013). Second, overall KC excitability is regulated by
66 feedback inhibition from a GABAergic neuron, MB-APL, that arborizes throughout
67 the MB (Papadopoulou et al., 2011, Lin et al., 2014a, Tanaka et al., 2008, Liu and
68 Davis, 2009). Thus only a small subset of KCs respond to a given sensory stimulus

69 (Perez-Orive et al., 2002, Turner et al., 2008, Honegger et al., 2011, Murthy et al.,
70 2008). Upon this representation of the sensory world, dopaminergic or
71 octopaminergic neurons convey information of punishment or reward and induce
72 memories that associate the sensory stimulus with its valence (Schroll et al., 2006,
73 Schwaerzel et al., 2003, Liu et al., 2012, Burke et al., 2012, Riemensperger et al.,
74 2005, Mao and Davis, 2009, Heisenberg, 2003, Claridge-Chang et al., 2009).

75

76 The functional architecture of the MB circuit is best understood in adult Drosophila
77 (Figure 1) (Ito et al., 1998, Lin et al., 2007, Tanaka et al., 2008, Strausfeld et al., 2003,
78 Crittenden et al., 1998, Ito et al., 1997, Aso et al., 2014a, Pech et al., 2013). In each
79 MB, the parallel axonal fibers of ~2,000 KCs can be divided into 16 compartmental
80 units by the dendrites of 21 types of MB output neurons (MBONs) and the axon
81 terminals of 20 types of dopaminergic neurons (DANs). A large body of behavioral
82 and physiological studies suggests that these anatomical compartments are also
83 parallel units of associative learning (see, for example, (Hige et al., 2015a, Lin et al.,
84 2014b)). In each compartment, the dendrites of a few MBONs overlap with axon
85 bundles of hundreds of KCs. Punishment and reward activate distinct sets of DANs.
86 DAN input to a compartment has been shown to induce enduring changes in efficacy
87 of KC>MBONs synapses in those specific KCs that were active in that compartment
88 at the time of dopamine release (Hige et al., 2015a). The valence of the memory
89 appears to be determined by which compartment receives dopamine during
90 training, while the sensory specificity of the memory is determined by which KCs
91 were active during training (Liu et al., 2012, Heisenberg, 2003, Burke et al., 2012).

92

93 Compartments can have distinct rates of memory acquisition and decay, and the 16
94 compartments together appear to form a set of parallel memory units whose
95 activities are coordinated through both direct and indirect inter-compartmental
96 connections (Aso and Rubin, 2016, Cohn et al., 2015, Perisse et al., 2016, Aso et al.,
97 2014a). The DANs which project to the $\alpha 1$ compartment, the ventral-most
98 compartment of the vertical lobe (Figure 1), play a key role in formation of
99 appetitive long-term memory of nutritional foods (Yamagata et al., 2015). DANs

100 which project to the other α lobe compartments, α 2 and α 3, play roles in aversive
101 long-term memory (Aso and Rubin, 2016, Sejourne et al., 2011, Pai et al., 2013). All
102 three of these compartments receive feedforward inputs from GABAergic and
103 glutamatergic MBONs whose dendrites lie in other MB compartments (Aso et al.,
104 2014a) known to be involved in aversive or appetitive memory (Aso and Rubin,
105 2016, Aso et al., 2010, Burke et al., 2012, Perisse et al., 2016). In addition, two types
106 of MB-intrinsic neurons send arbors throughout the MB-lobes: a large GABAergic
107 neuron, MB-APL, which provides negative feedback important for sparse coding
108 (Papadopoulou et al., 2011, Lin et al., 2014a), and the MB-DPM neuron, which is
109 involved in memory consolidation and sleep regulation (Waddell et al., 2000, Keene
110 et al., 2006, Haynes et al., 2015, Yu et al., 2005a, Cervantes-Sandoval and Davis,
111 2012, Keene et al., 2004).

112
113 Previous EM studies in the mushroom body lobes of cockroaches (Mancini and
114 Frontali, 1970, Mancini and Frontali, 1967), locusts (Leitch and Laurent, 1996),
115 crickets, ants, honey bees (Schurmann, 1974, Schurmann, 2016), and Drosophila
116 (Technau, 1984) identified KCs by their abundance, fasciculating axons and small
117 size. Additionally, Leitch and Laurent (1996) identified large GABA immunoreactive
118 neurons that contact KC axons in the locust pedunculus. While these data provided
119 early insights to guide modeling of the MB circuit, the volumes analyzed were
120 limited and most neuronal processes could not be definitively assigned to specific
121 cell types. In this paper, we report a dense reconstruction of the three
122 compartments that make up the α lobe of an adult Drosophila male (Figure 1).
123 Because we performed a dense reconstruction, with the goal of determining the
124 morphology and connectivity of all cells in the volume, we have confidence that we
125 have identified all cell types with processes in the α lobe.

126
127 Comprehensive knowledge of the connectivity in the α lobe has allowed us to
128 address several outstanding issues. The first concerns the nature of KC>MBON
129 connectivity. While each KC passes through all three compartments, it is not known
130 if individual KCs have *en passant* synapses in each compartment. Thus it remains an

131 open question whether the sensory representation provided to each compartment
132 and each MBON within a compartment is the same or whether different MBONs
133 within a compartment might sample from non-overlapping sets of KCs, and thus use
134 independent sensory representations for learning. It was also not known which, if
135 any, other cell types are direct postsynaptic targets of KCs.

136

137 The second concerns dopamine modulation. What are the locations of
138 dopaminergic synapses and what does this distribution imply about the targets of
139 dopaminergic modulation as well as volume versus local transmission? Cell-type-
140 specific rescue of dopamine receptor mutants suggests that dopamine acts
141 presynaptically in the KCs of KC>MBON synapses (Kim et al., 2007, Qin et al., 2012a,
142 Liu et al., 2012, Ichinose et al., 2015). However postsynaptic mechanisms have also
143 been proposed (Cassenaer and Laurent, 2012, Pai et al., 2013) and a recent study
144 detected expression of dopamine receptors in MBONs (Crocker et al., 2016), raising
145 the possibility that MBONs might also be direct targets of DAN modulation.

146 Behavioral, imaging and electrophysiological data (Aso et al., 2010, Hige et al.,
147 2015a, Cohn et al., 2015) indicates that dopamine modulation respects the borders
148 between compartments, but we do not know whether these borders have a distinct
149 structure, such as a glial sheet.

150

151 The third concerns the two MBON types that send feedforward projections into the
152 α lobe. These MBONs have important roles in associative learning as revealed by
153 behavioral assays and have been postulated to integrate memories of opposing
154 valence and different time scales (Aso et al., 2014a, Aso and Rubin, 2016, Aso et al.,
155 2014b, Perisse et al., 2016). However, we do not know which cell types these
156 feedforward MBON projections targets within the MB.

157

158 The fourth concerns the two neurons, MB-APL and MB-DPM, which arborize
159 throughout the MB and are thought to regulate MB function globally (Liu and Davis,
160 2009, Lin et al., 2014a). What is their local synaptic connectivity within the α lobe
161 and what can this tell us about how they perform their roles?

162
163 Finally, the three compartments of the α lobe differ in important aspects, including
164 valence of the memory formed, the time course of memory formation and retrieval,
165 and the numerical complexity of their DAN inputs and MBON outputs. Are there
166 obvious differences in the microcircuits of different compartments?
167
168 In this paper, we report the answers to these questions. In addition, we demonstrate
169 the utility of detailed anatomy at the electron microscopic level to provide novel
170 insights: We show that nearly all cell types in the α lobe contain more than one
171 morphological class of synaptic vesicle, raising the possibility that these cells utilize
172 multiple neurotransmitters. In addition, we describe two prevalent sets of synaptic
173 motifs—from DANs to MBONs and from KCs to DANs—that were unanticipated
174 despite the extensive anatomical, physiological, behavioral and theoretical studies
175 that have been performed on the insect MB. We characterize these novel DAN to
176 MBON connections using behavioral and physiological assays and find that DAN
177 activation produces a slow depolarization of postsynaptic MBONs and can weaken
178 memory recall.
179

180 **Results**

181

182 **Data acquisition, segmentation and proofreading**

183

184 The brain of a five-day-old adult male fly was fixed, embedded and trimmed as
185 described in Methods. A ~40 x 50 x 120 μm volume (Figure 1B) encompassing the
186 vertical lobe of the MB was imaged by focused ion-beam milling scanning electron
187 microscopy (FIBSEM) (Xu et al., 2017) over a five week imaging run (Videos 1 and
188 2). The assembled volume has isotropic voxels (8 x 8 x 8 nm) allowing image data to
189 be viewed with the same resolution along any axis.

190

191 The portion of the imaged volume that contained the α lobe was identified based on
192 the morphologies of the KCs and ensheathing glia. We then reconstructed the
193 shapes of the individual neurons in this selected volume, as well as mapped the
194 locations of synapses. This process entailed the application of machine vision
195 algorithms for synapse detection and image segmentation—that is, assigning each
196 voxel to a particular neuron. These procedures have been previously published
197 (Takemura et al., 2015, Plaza et al., 2014, Parag et al., 2014) and are briefly
198 described in Methods. The results of these automated processes were then
199 reviewed and edited by trained human proofreaders; a total of ~8 person years was
200 devoted to proofreading. The neuronal processes that entered or left the α lobe
201 were traced until they exited the imaged volume; this information was helpful in
202 distinguishing cell types, as described below.

203

204 **Cell type identification**

205

206 Because of the constrained size of the imaged volume, only the portions of the
207 neurons that have processes in the α lobe were reconstructed. To identify the cell
208 type of each partially reconstructed cell in the EM volume we compared their
209 morphologies to existing images of the relevant MB cell types from light microscopy

210 (Figure 2)(Aso et al., 2014a). Our confidence in our ability to make correct
211 correspondences by this approach was increased by the completeness of both EM
212 and light microscopy datasets. We found only one cell type in our EM
213 reconstructions that had not been described at the light level, a single MBON that we
214 named (MBON- α 2sp). All the other reconstructed arbors could be assigned to one of
215 the neurons previously identified at the light level (Figures 2 and 3) except in the α 1
216 compartment, where we reconstructed a few arbors that were not large enough to
217 allow unambiguous assignment based on comparing light and EM morphologies and
218 whose branches exited the imaged volume before connecting to an identified cell.
219 Based on comparison with light microscopic anatomy (Aso et al., 2014a), we expect
220 that these are segments of APL, DPM and MBON- γ 1pedc> α/β (see below). One other
221 difference between the observed light and EM morphologies was that MBON- α 2p3p
222 extends a few dendrites into α 3 based on light microscopic analyses (Aso et al.
223 2014a), whereas in our EM reconstruction of this cell we found dendritic
224 arborizations were confined to α 2.

225
226 We reconstructed 949 KCs in the α lobe, a number that agrees well with the
227 previous estimate of ~1,000 α/β KCs obtained by counting genetically labeled cell
228 nuclei with light microscopy (Aso et al., 2009). The α lobe KCs have been divided
229 into three classes based on the location of their axons in the lobe: posterior (α/β p),
230 surface (α/β s) or core (α/β c) (Tanaka et al., 2008, Strausfeld et al., 2003, Lin et al.,
231 2007). The α/β p cells are clearly distinct in both morphology and synaptic
232 connectivity (see below) and we assigned 78 neurons to this class, compared to ~90
233 estimated by Aso et al. (2014a). The remaining α/β s and α/β c KCs form a set of
234 concentric layers in the α lobe arranged by birth order, with KCs that are born more
235 recently occupying the more central, or core, layers. Following established
236 nomenclature, we refer to KCs that occupy the outer most layer of the α lobe as
237 surface, α/β s, and those occupying the inner layers as core, α/β c; the core KCs can
238 be further divided into inner-core, α/β c(i) and outer-core, α/β c(o) (Tanaka et al.
239 2008). When the distinction is unimportant, we simply refer to the non-posterior

240 KCs collectively as α/β sc. The relative spatial arrangements of these KC classes is
241 illustrated in Figure 2A, Figure 3A and Video 3.

242

243 The α lobe, a linear structure formed by the continuous axons of the KCs, can be
244 divided into three non-overlapping compartments, α 1, α 2 and α 3 (Figures 1 and 2).
245 Each compartment has a unique set of DANs and MBONs whose complex dendritic
246 arbors demarcate the extent of the compartment (Figure 1; Video 4). The α 3
247 compartment at the tip of the α lobe contains two PPL1- α 3 DANs and two MBON- α 3
248 cells (Figure 2G and 2H). The α 2 compartment has two PPL1- α' 2 α 2 DANs (neurons
249 that innervate both the α 2 compartment and the α' 2 compartment of the α' lobe)
250 and four MBONs of three distinct types that differ based on the KCs they receive
251 input from: one MBON- α 2sc, two MBON- α 2p3p and one MBON- α 2sp (Figure 2I-L).
252 The α 1 compartment has 16 PAM- α 1 DANs and two MBON- α 1 cells (Figure 2M-O;
253 Video 5). These cell numbers are per hemisphere for MBONs but per brain for DANs
254 because each DAN innervates the MB in both hemispheres. In some cases, the
255 distinction of arbors of the MBONs and DANs were not very clear in each
256 compartment. In these cases, we used the characteristic axonal positions at which
257 the neurites of these cells enter the MB lobes (Aso et al., 2014a) in making cell-type
258 assignments. For example: PPL1- α 3's main axons all enter the lobe from the
259 posterior side whereas MBON- α 3's axons enter from the medial side. DPM has a
260 thick main axon entering into the α lobe from the posterior medial side (Waddell et
261 al., 2000)(See Figure 3-figure supplement 1 in Aso et al. 2014a) whereas APL has a
262 very thin axon entering the vertical lobe from the posterior side. Further
263 confirmation for the identities of the cell types assigned to these reconstructed
264 arbors was provided by their distinct synaptic connectivity. For example, early in
265 the process we found MBON dendritic arbors had no pre-synaptic sites, APL was
266 pre-synaptic to KCs but not DANs, and DPM was pre-synaptic to both. These
267 patterns enabled us to double-check the assignments that we had made based on
268 morphology.

269

270 There are six additional cells with arbors in the α lobe, and each innervates all three
271 compartments (Figure 2B-F): the ipsilateral APL and DPM, MB-intrinsic neurons
272 that arborize widely throughout the MB lobes; a neuron expressing the
273 neuropeptide SIFamide that arborizes broadly throughout the brain (Park et al.,
274 2014, Verleyen et al., 2004); and the axons of the ipsilateral MBON- $\beta 1>\alpha$ and the
275 ipsi- and contralateral MBON- $\gamma 1pedc>\alpha/\beta$, which project from other MB lobes. In
276 total, we reconstructed and identified portions of 983 neurons in the α lobe. Since
277 we accounted for all major neurites and neuronal profiles and had only small
278 fragmented bodies left unassigned to a specific neuronal type in the reconstructed
279 volume (see below for the quantitative estimate), we are confident that there are no
280 other cell types with significant arborization in the α lobe.

281

282 **Synapse number and morphology**

283

284 The resolution provided by EM allowed us to determine the number and location of
285 chemical synapses between the cells we identified, information that was not
286 available from previous light level analyses. We identified 89,406 presynaptic
287 densities (Figures 4 and 5), using a combination of machine learning algorithms and
288 human annotation. We then manually annotated a total of 224,697 postsynaptic
289 sites in the α lobe, based primarily on their adjacency to a presynaptic density (see
290 Methods). Of these postsynaptic sites, 93% could be traced back to the main arbors
291 of an identified cell. The remaining 7% of postsynaptic sites were typically in small
292 branches that could not be reliably traced to a particular cell; the small size and
293 discontinuous nature of these neurites indicates that they are fragments of
294 identified cells rather than collectively constituting an additional cell type. For 86%
295 of synapses, we were able to identify the cell types of both the pre- and postsynaptic
296 cells. The fact that we did a dense reconstruction, mapping the vast majority of
297 synapses, allowed us to determine quantitative properties of the network of
298 neuronal connections that would not be revealed by a sparser sampling approach.

299

300 Figure 4 shows examples of the synaptic morphologies we observed in the MB α
301 lobe, and Figure 5 shows examples from a higher quality dataset (with 4 x 4 x 4 nm
302 voxels and imaged with higher signal to noise) collected from selected regions of a
303 second brain. While the \sim 100x slower imaging required to collect data at this
304 higher resolution precluded imaging the entire volume, these selected areas allowed
305 us to catalog the various synaptic motifs present in the MB with greater confidence.

306

307 Each MBON receives thousands of synapses from KCs in each compartment and we
308 frequently observed two or more KCs making adjacent synapses onto a dendritic
309 process of an MBON, often making rosette-like structures that can also include DAN
310 synapses (Figures 4A-C and 5A, B; Video 6). For the purpose of this analysis, we
311 define a convergence as a tight grouping (within 300 nm) of two KCs pre-synaptic to
312 a common target, and a rosette as a convergence that includes a distinct density at
313 their point of KC to KC contact, which we have interpreted—based solely on
314 morphology—as reflecting potential reciprocal synaptic contact between the KCs
315 (KC $<\!\!>$ KC). Convergences and rosettes were found for every cell type that is post-
316 synaptic to KCs, but the fraction of synapses to a given cell type that occurred in
317 these structures varied between cell types. The highest percentage observed was
318 for KC>MBON synapses, where 80-93% (depending on the MBON) of the 54234 KC
319 pre-synaptic sites that connect to MBONs are part of a convergence and 62% part of
320 a rosette. Video 7 shows how rosettes and sites of convergence as well as single
321 inputs are distributed along the MBON dendrite. Other KC targets had a lower
322 fraction of their synapses to KCs in rosettes: KC>DAN (60% convergence, 37%
323 rosettes of 9615 pre-synaptic sites); APL (69% convergence, 32% rosettes of 9063
324 pre-synaptic sites); and SIF (44% convergence, 35% rosettes of 68 pre-synaptic
325 sites). For DPM, in contrast, although 56% of its 7168 KC>DPM synapses were part
326 of a convergence, only 12% were part of a rosette. Of KC>KC synapses, 55% occur
327 in rosettes. We asked whether two KCs that participated in a rosette had an
328 increased chance of converging again in a second rosette elsewhere in the α lobe;
329 we found no such correlation.

330

331 Both clear and dense core synaptic vesicles (DCVs) were observed in early EM
332 studies on the cockroach mushroom body (Mancini and Frontali, 1970, Mancini and
333 Frontali, 1967). Similarly, we found that the presynaptic sites of all reconstructed
334 cell types except the SIFamide neuron contain at least two morphologically distinct
335 classes of synaptic vesicles (Table 1; Figure 5E), suggesting that most cell types in
336 the MB use multiple neurotransmitters. SIFamide neurons contain only large dense-
337 core vesicles (roughly 125 nm in diameter), while all other cells contain both DCVs
338 and 45 nm diameter clear synaptic vesicles (Figure 5E; Table 1). The DCVs are 80
339 nm diameter in KCs, PPL1- $\alpha'2\alpha 2$, PAM- $\alpha 1$, MBON- $\beta 1>\alpha$, APL, and DPM, while those
340 in PPL1- $\alpha 3$ are larger with a diameter of close to 100 nm (Table 1). We found
341 relatively few DCVs in APL, and almost none in MBON- $\gamma 1pedc>\alpha/\beta$ (Table 1).
342 Because the MBONs with dendrites in the α lobe (MBON- $\alpha 1$, MBON- $\alpha 3$, MBON- $\alpha 2sc$,
343 MBON- $\alpha 2p3p$ and MBON- $\alpha 2sp$) do not have pre-synaptic sites within the
344 reconstructed volume, we do not have information on what type(s) of vesicles they
345 contain.

346

347 The identification of synapses is based purely on morphology. Presynaptic densities
348 in Drosophila generally have a characteristic T-shaped specialization, the T-bar
349 ribbon (Shaw and Meinertzhagen, 1986). Most KC synapses, however, have
350 elongated-shaped presynaptic densities rather than typical T-bars. While these are
351 readily identified (see Figures 4 and 5), we cannot exclude the possibility that large
352 DCVs that fall near a membrane could occasionally be mistaken for a presynaptic
353 density. Postsynaptic densities are more difficult to recognize in the lower
354 resolution (8 x 8 x 8 nm voxel) FIB-SEM dataset and thus in most cases postsynaptic
355 targets have been identified solely by their apposition to presynaptic sites. Another
356 limitation of the current work is that we are unable to detect gap junctions,
357 structures that can provide electrical coupling between cells and contribute to
358 circuit function (Wu et al., 2010, Liu et al., 2016, Marder et al., 2016). A file
359 containing all synapse locations is provided as Supplemental File 1.

360

361 **Delivery of sensory information**

362
363 We found that each of the three compartments has access to similar sensory
364 information. As KC axons pass through the compartments, every KC makes multiple
365 *en passant* synapses in each compartment (Figure 5C, D; Table 2; Videos 8, 9 and
366 10).

367
368 The α_3 and α_1 compartments each have two MBONs of similar morphology whose
369 dendritic arbors fill the entire compartment. The distribution of the number of
370 synapses each KC makes with these MBONs is shown in Figure 4-figure supplement
371 1. Every KC made synapses onto each of these MBONs, averaging 28 ± 8 in the α_3
372 compartment and 20 ± 6 in α_1 . The sole exception was a single KC whose axon did
373 not project all the way to the α_3 compartment; its uniqueness suggests that it was a
374 developmental aberration. Interestingly, the data showed a close match to a Poisson
375 distribution, as expected if each KC>MBON synapse is formed during development
376 without regard to the placement of other KC synapses on the same MBON (Figure 4
377 – figure supplement 1). A simple Poisson model predicts the distribution of synapse
378 counts (how many KCs have no synapses to the target, how many have one, how
379 many have two, etc.) from the total number of KCs (M) and the total synapse count
380 (N). The expected number c of KCs with k connections is

$$c = N \frac{(N/M)^k}{k!} e^{-N/M}$$

381 There are no free parameters, and the variance is equal to the expected
382 number. Despite the fact we could find little statistical structure to describe the
383 synaptic connectivity, KC>MBON convergence was nevertheless high enough that
384 these MBONs appear to integrate information from every KC and all KC classes that
385 are found in their compartment.

386
387 In contrast to α_1 and α_3 , where each MBON has a compartment-filling dendritic
388 arbor, α_2 has three distinct types of MBONs (two MBON- α_2p3p neurons, one
389 MBON- α_2sc and one MBON- α_2sp) whose dendrites arborize in different subregions
390 of the compartment (Figure 2J-L). Accordingly, they differ significantly in their

relative inputs from different KC classes (Table 2; Figure 6A). For example, MBON- α 2p3p receives more than 75% of its input from α/β p KCs, which constitute only 8% of α lobe KCs. Interestingly, the α/β p KCs are not activated by odors (Perisse et al., 2013) and the α/β p dendrites are physically separated from those of odor-responding KCs (Lin et al., 2007, Tanaka et al., 2008). On the other hand, MBON- α 2sc receives inputs almost exclusively from α/β sc KCs whose dendrites lie in the main calyx and receive inputs primarily from olfactory projection neurons. Thus, our reconstructions indicate that MBON- α 2p3p and MBON- α 2sc have a strong bias in how they sample modalities of sensory information. Despite this biased sampling, MBONs that project extensively to a particular sub-region connect to every KC within that subregion (Table 3). However, the borders between subtypes of KCs, especially between α/β s and α/β c KCs, are not crisp and some MBONs receive a fraction of their inputs from outside their primary innervation zone; in these cases, the number of KC>MBON synapses made by individual KCs is also typically lower. The fact that the sub-classes of KCs defined by connectivity do not exactly coincide with the sub-classes we defined by morphology results in a few exceptions to a Poisson distribution of KC>MBON synapses (Figure 4 – figure supplement 1); for example, MBON- α 2sp only receives input from the outermost half of the core KCs.

Other features of the wiring statistics also suggest that individual neurons make their connections during the development of the MB with little or no consideration of other cell's connections. For example, the number of synapses each KC makes onto one of the MBONs in a compartment is a poor predictor of the number of connections with the second MBON. More specifically, there are two MBONs in both the α 3 and α 1 compartments and each of the two MBONs in a compartment received similar numbers of KC synaptic contacts, but the number of contacts that an individual KC makes to the two MBONs in a compartment was not highly correlated (Pearson's r of 0.01, 0.21 and 0.27 for α 3, Kc-s, KC-c, and KC-p, and 0.00, 0.21, and 0.41 in α 1 for the same subsets. See Methods). Similarly, we found that when two DANs of the same type each connect to a subset of KCs, those subsets

421 appear to be independent, neither seeking nor avoiding common partners. For
422 example, the two PPL1- $\alpha'2\alpha 2$ DANs each connect to about half of the KCs in the $\alpha 2$
423 compartment (52.3% and 49.6%), while 23.5% of KCs connect to neither and 25.4%
424 to both; thus their patterns of connection are not significantly different from
425 independent (Fisher exact test, $P=0.7$). Indeed, we found no evidence for the
426 individual members of a pair of cells of the same type influencing each other's
427 wiring. Additionally, connections to one KC do not appear to influence connections
428 to other KCs. For example, consider the connections from PPL1-05-A to the
429 posterior KCs, where are 151 synapses in total to the 78 KCs. In the case where
430 wiring occurs without inherent preferences, Poisson statistics predicts that (on the
431 average) 11.1 ± 3.4 KCs will have no synapses, 21.8 ± 4.7 will have 1 synapse,
432 21.1 ± 4.7 KCs will have 2, 13.6 ± 3.7 KCs will have 3, and so on. The actual counts are
433 10,23,24,12,3,4,2, agreeing well ($\chi^2 = 5.3$ for 7 degrees of freedom) with the model.
434

435 **Distribution of modulatory input**

436

437 Reconstructions of dopaminergic input to the α lobe showed that these cells make
438 synaptic contacts with a variety of postsynaptic partners, including axo-axonal
439 contacts with the presynaptic terminals of KCs. The projection sites of the DANs in
440 each compartment are plotted in Figure 6B. They primarily target KCs, but
441 surprisingly also make many contacts with MBONs. In contrast, the DANs make far
442 fewer synapses with the other neurons in the lobes, APL and DPM.
443

444 Given the increased dopamine receptor expression in the MB, DAN>KC synapses
445 have long been postulated to exist (Han et al., 1996, Kim et al., 2003).
446 Morphologically, they are polyadic, and in some cases occur with the participating
447 DAN, KC and MBON in close proximity (see, for example, Figure 4D). While KCs are
448 the main target of DANs, DAN>KC synapses are far fewer than KC>MBON synapses,
449 numbering only about 10% by comparison (Tables 2 and 4). In fact, only 6% of
450 KC>MBON synapses (3825 out of 61486) have a DAN terminal within a radius of

451 300 nm. Despite this, electrophysiology data indicate that DANs induce strong
452 synaptic depression at the KC>MBON synapse, suggesting that the great majority of
453 synapses are affected (Hige et al. 2015a) and, in turn, implying that the
454 dopaminergic modulation of KC>MBON synapses occurs by volume, rather than
455 local, transmission of dopamine. Consistent with this view, the nearest DAN>KC
456 synapse can often be distant from a given KC>MBON synapse; on average, the
457 closest DAN>KC synapse falls outside a radius of 800 nm from the given KC>MBON
458 synapse, with more than 10 other synapses (typically KC>KC, KC>MBON or
459 KC>DAN) interspersed. Moreover, while every KC makes multiple synapses onto
460 the MBONs in each compartment (Table 3), not all KCs receive synaptic input from a
461 DAN (Table 4). For example, in α 2, 23.5% of the KCs lack synapses from a DAN.
462

463 The α 3 and α 2 compartments are each innervated by a pair of PPL1 cluster DANs,
464 one ipsilateral and one contralateral, which arborize throughout the compartment.
465 Thus, in α 2, while the distinct MBON cell types sample differently from KC subtypes,
466 all KC>MBON synapses receive dopaminergic input from the same DANs, suggesting
467 that they are coordinately modulated. In contrast, α 1 receives modulatory input
468 from 16 PAM cluster DANs whose individual arbors are more restricted (Figure 2N;
469 Table 4; see also Video 5) leaving open the possibility that KC-sc>MBON synapses
470 are modulated differentially to KC-p>MBON synapses.

471
472 Previous work indicates that dopaminergic modulation respects the border between
473 compartments (Hige et al., 2015a). However, we saw no obvious boundary
474 structure in our EM images, such as a glial sheet, that might block dopamine
475 diffusion. Light microscopic studies of glia in the adult brain likewise show an
476 apparent absence of glial boundaries between MB compartments (Kremer et al.,
477 2017). To explore whether the observed functional compartmentalization could be
478 achieved without a discrete boundary, we estimated the predicted extent of cross-
479 compartment modulation under various assumptions of the range of dopamine
480 diffusion (Figure 4-figure supplement 2). For example, these calculations showed

481 that, if the effective range of dopamine action was 2.5 microns from its release site,
482 99% KC>MBON synapses in the same compartment, but only 1% in the neighboring
483 compartment, would be close enough to be modulated by a compartment-specific
484 DAN. This suggests that a discrete inter-compartment boundary may not be
485 required.

486

487 **Connectivity of the intrinsic neurons APL and DPM**

488

489 The APL and DPM neurons innervate the MB lobes in their entirety and are thought
490 to modulate overall MB function (Tanaka et al., 2008, Waddell et al., 2000, Liu and
491 Davis, 2009, Lin et al., 2014a, Pitman et al., 2011, Haynes et al., 2015, Lee et al., 2011,
492 Keene et al., 2006). APL is an inhibitory neuron that governs overall levels of
493 activity across the KC population to maintain the sparseness of the odor
494 representation (Papadopoulou et al., 2011, Lin et al., 2014a). The DPM neuron is
495 immunoreactive to the *amnesiac* neuropeptide (Waddell et al., 2000) and has been
496 proposed to use serotonin (Lee et al., 2011) and GABA (Haynes et al., 2015) as
497 neurotransmitters; its role in the circuit is less clear, but it is gap-junctionally
498 coupled to APL (Wu et al., 2011), and appears to be important for memory
499 consolidation (Yu et al., 2005a, Pitman et al., 2011, Keene et al., 2006, Keene et al.,
500 2004). The profile of DPM's and APL's input connectivity is shown in Figure 6A and
501 Table 5. Both cell types get many inputs from KCs, which would allow them to
502 evaluate the overall activity in the MB. They both also receive input from DANs in
503 all three compartments (Table 5), however these were far fewer than the number of
504 synapses the DANs made onto the MBONs in each compartment (Table 6).
505 Nevertheless, they may still be subject to dopamine modulation, given the potential
506 diffusion distance of dopamine; it is not known whether APL or DPM express
507 dopamine receptors.

508

509 In terms of their output, both cells primarily interact with the KCs (Figure 6B). In
510 fact, APL sends no output to any DANs and no MBONs other than a few connections
511 to MBON- α 1 (Table 5). Thus, APL's role seems largely confined to influencing the

512 sensory input the KCs convey to the lobes. On the other hand, DPM makes synapses
513 onto MBONs and DANs in all three α -lobe compartments (Table 5). Overall the
514 output profiles of these cells were quite similar across all three compartments. The
515 only exception to this was the high number of connections we observed between
516 DPM and the two MBON- α 1s (Table 5); while the role of these connections is
517 unclear, we note that DPM has been shown to play a role in consolidation of long
518 term appetitive memory (Krashes and Waddell, 2008), a process that takes place in
519 the α 1 compartment (Ichinose et al., 2015).

520
521 One surprising finding from our reconstructions that was not visible from confocal
522 imaging of these cells was that both DPM and APL have modular anatomy. The DPM
523 arbor splits outside the MB lobe into three large branches which ramify within
524 distinct zones of the α lobe; one branch innervates α 1 and two others α 2 and α 3
525 (color-coded in Figure 2E). The zones defined by these branches might serve as
526 independent information processing domains and could explain the observation
527 that aversive learning-related changes in calcium signals in DPM were confined to
528 the vertical branch of this neuron (Yu et al., 2005b). In contrast, APL sends a series
529 of separate processes that project through the α lobe, but these individual branches
530 are not connected inside the α lobe (Video 11). These processes may each serve as
531 discrete units of local inhibitory feedback in the lobes.

532

533 **Unanticipated circuit motifs**

534

535 In addition to the circuit motifs anticipated from prior anatomical, behavioral and
536 physiological studies (Heisenberg, 2003, McGuire et al., 2005, Waddell, 2013, Hige et
537 al., 2015a, Cohn et al., 2015, Owald et al., 2015), our comprehensive reconstruction
538 shed light on some synaptic connections that have not been extensively studied or,
539 in some cases, previously described. For example, we found additional postsynaptic
540 targets for KCs beyond the canonical KC>MBON synapse. Most strikingly, KCs made
541 direct synaptic connections to DANs (Figure 4E; Table 7). Indeed, the number of
542 KC>DAN synapses is larger than the number of DAN>KC synapses (5037 vs. 2984 in

543 α 3; 1599 vs. 1466 in α 2; and 3054 vs. 2012 in α 1).

544

545 We also frequently observed structures that we interpret to be KC to KC synaptic
546 connections (Figures 4C and 5A, B; Table 8); such synapses have been previously
547 described in the locust MB (Leitch and Laurent 1996). Most such KC to KC
548 connections occur as a part of more complex structures: a presynaptic density
549 associated with a KC>KC synapse usually has at least one additional postsynaptic
550 partner. The most frequent partner is an MBON and in 70-85% of cases (depending
551 on compartment) both KCs synapse onto the same MBON dendrite forming a
552 KC<>KC>MBON triangular motif as shown in Figures 5A and 5B. The distribution of
553 postsynaptic cell types are similar in such KC<>KC>cell type and simple KC>cell
554 type structures.

555

556 Finally, we discovered that DANs make direct synaptic outputs to the MBONs, a
557 novel circuit motif that we found in all three compartments (Figure 4D; Table 6;
558 Video 6). The number of DAN>MBON synapses was small compared to that of
559 KC>MBON synapses—only 2 to 8% of that number, depending on the MBON.
560 However, the fraction of KCs that are active at any one time is limited by sparse
561 coding and has been estimated to be ~6% (Campbell et al., 2013, Turner et al.,
562 2008). Thus, if all the synapses from a single DAN are active, then the total active
563 synaptic input that an individual MBON would receive from DANs and KCs might be
564 comparable. This prompted us to carry out physiological and behavioral
565 experiments to explore the functional significance of this novel circuit motif.

566

567 **Direct DAN to MBON synaptic transmission**

568

569 We asked if the observed DAN to MBON connections served to provide direct
570 synaptic transmission from DANs to MBONs. We used the α 1 compartment for these
571 experiments largely for technical reasons: we had the split-GAL4 and LexA drivers
572 required for imaging and photostimulation and the cell body of MBON- α 1 is
573 accessible for patch clamping. We photostimulated PAM- α 1, using the light-gated

574 cation channel Chrimson-tdTomato (Klapoetke et al., 2014), while imaging calcium
575 responses in the dendrites of the MBON- α 1 with GCaMP6s in explanted brains
576 (Figure 7A). A 100 msec photostimulation of PAM- α 1 evoked a slow calcium rise in
577 the MBON- α 1 (Figure 7B). It took a few seconds for GCaMP fluorescence to reach
578 peak amplitude, which then slowly decayed over ~20 seconds.

579

580 Similar responses were observed with electrophysiological recordings from an *in*
581 *vivo* preparation (Figure 7C, D). With whole-cell recordings from MBON- α 1, we
582 observed that a 2 msec photo-stimulation of PAM- α 1 also evoked a slow
583 depolarization, of sufficient amplitude to elicit a spiking response. To test if these
584 excitatory connections from DAN to MBON are direct, we blocked action potential
585 propagation with tetrodotoxin (1 μ M) and cholinergic transmission with
586 mecamylamine (250 μ M). These blockers minimize the possibility that DANs exert
587 their effect on the MBONs via intervening neurons, such as KCs, which have been
588 shown to be cholinergic (Yi et al., 2013, Barnstedt et al., 2016). Indeed, we observed
589 no significant MBON response to direct KC stimulation in these conditions (Figure 7
590 – figure supplement 1), consistent with the results of (Barnstedt et al., 2016). In
591 contrast, DAN stimulation in the same conditions elicited a slow depolarizing
592 response (Figure 7C, D), indicating that there is monosynaptic excitatory
593 transmission from DAN to MBON. In fact, there was a tendency for the response to
594 become even larger, and the decay kinetics even slower in the presence of blockers.
595 This may reflect changes in the sensitivity of dopaminergic signaling, as
596 spontaneous activity of PAM- α 1 may hold the signaling cascade in a partially
597 desensitized state (Ichinose et al., 2015), which is then alleviated by the blockers.
598 The response was strongly (although not completely) diminished by the addition of
599 a D1 dopamine receptor antagonist (Figure 7E, F), indicating that DAN>MBON
600 transmission acts largely through dopamine receptors (Boto et al., 2014, Sitaraman
601 et al., 2015)(Boto et al., 2014 Sitaraman et al., 2015). Indeed previous work has
602 shown that MBONs express dopamine receptors, but at lower levels than KCs
603 (Crocker et al., 2016). However, as discussed above, we observed that DANs have at

604 least two morphologically distinct types of presynaptic vesicles, and we cannot
605 exclude the possibility that a co-transmitter contributes to the effects we observe
606 here. Nor do we rule out the possibility that dopamine released from other DAN
607 synapses diffuses to the sites of direct DAN-MBON contact, although we did not see
608 any evidence for multiphasic kinetics in the response. Nonetheless, our experiments
609 revealed direct, slow excitatory synaptic signaling between DANs and MBONs in α 1,
610 providing direct physiological support that the DAN to MBON synapses we observed
611 in our EM reconstructions are functional.

612

613 **A possible behavioral role for DAN to MBON synapses**

614

615 Our finding that DANs directly synapse on MBONs implies that DANs can affect the
616 activity of MBONs in at least two ways: (1) by modulating KC to MBON synapses,
617 which provides a lasting record of coincident activation of specific KCs and DANs;
618 and (2) by direct synaptic transmission to MBONs, whereby the DANs can
619 immediately convey information about the current state of the environment. Based
620 on the population coding model of how the activity of individual MBONs is
621 integrated to bias behavior (Aso et al., 2014b), we would expect that activation of an
622 individual DAN and the resulting activation of its target MBONs could have a
623 significant effect on behavior.

624

625 As a simple test of this idea, we first optogenetically trained animals to form an
626 appetitive association with a specific odor by pairing activation of PAM- α 1 with
627 odor presentation. We then tested the effects of activating PAM- α 1 during memory
628 recall 1 min after training. We found that activation suppressed the conditioned
629 approach response to the odor (Figure 8A, B). Similarly, when we examined the
630 effects on memory recall with a 1-day old memory from optogenetic training in the
631 α 3 compartment, we again found DAN activation suppressed expression of the
632 induced aversive memory (Figure 8C). While DANs activation in the absence of
633 odors can promote forgetting (Berry et al., 2012), memories in α 1 and α 3 are
634 resistant to such treatment (Aso and Rubin, 2016). We also found that optogenetic

635 activation of PPL1- α 3 alone or in combination with other PPL1 DANs, in the absence
636 of odor presentation, produced an attraction response (Figure 8D).

637

638 Our finding that stimulating the DAN innervating a compartment while testing for
639 memory recall from that same compartment leads to a reduction in performance is
640 the expected behavioral phenotype, taking together the sign of action we found for
641 PAM- α 1 activation on MBON- α 1 output and our prior work on population coding of
642 valence by MBONs (Aso et al. 2014b). While this consistency with expectation is
643 reassuring, our optogenetic experiments cannot themselves distinguish the *in vivo*
644 roles of DAN signaling to MBONs, KCs or other cell types. They do, however, raise
645 the intriguing possibility that the observed reduction of the conditioned response to
646 an odor might provide a mechanism for integrating the ongoing activity of a DAN,
647 reporting on the current environment, and an associative memory induced by that
648 DAN's prior activity in the presence of the odor. More experiments will be required
649 to determine if such a strategy is employed by a fly under normal conditions.

650

651 **Feedforward MBONs**

652

653 There are two feedforward neurons that convey information from other lobes to
654 compartments within the α lobe, MBON- β 1> α and MBON- γ 1pedc> α / β (Figure 2B,
655 C)(Aso et al., 2014a, Aso and Rubin, 2016, Perisse et al., 2016). MBON- β 1> α
656 receives input from the β 1 compartment, which supports appetitive memory
657 formation (Perisse et al., 2013, Aso and Rubin, 2016), and sends axonal projections
658 throughout the α lobe. MBON- γ 1pedc> α / β conveys information from the γ 1pedc
659 compartment, where it supports aversive memory, and projects throughout both
660 the α and β lobes. It has been postulated that their feedforward outputs mediate the
661 interaction between memories with different time scales and valences (Aso and
662 Rubin, 2016, Aso et al., 2014b, Perisse et al., 2016). To explore the circuit
663 mechanisms that might govern this interaction, we examined the synaptic targets of
664 these feedforward neurons in the α lobe. We were able to do so except in the α 1

665 compartment where, for the technical reasons described above, we were unable to
666 identify the arbors of MBON- γ 1pedc> α/β (Figure 2C).

667

668 The most predominant targets of MBON- β 1> α and MBON- γ 1pedc> α/β were the
669 dendrites of the MBONs in each compartment, which receive ~100 synapses
670 generally as part of polyadic synapses where multiple postsynaptic elements are
671 associated with one presynaptic site (Figure 4F and 4G; Table 5; Video 6). While the
672 majority of inputs to each MBON come from KCs, as mentioned earlier the sparse
673 activity of KCs means that their input to the target MBONs is less than the number of
674 KC>MBON synapses implies. In contrast, MBONs respond to virtually all odors in
675 untrained flies (Hige et al., 2015b). Thus MBONs in the α lobe likely receive a
676 significant proportion of their input from feed forward MBONs and would be
677 expected to be sensitive to alterations in their activity.

678

679 The synapses of these feedforward MBONs showed an interesting spatial
680 distribution. In α 1, the terminals of MBON- β 1> α are concentrated on a region of the
681 MBON- α 1 dendrites closest to the cell's axon, a cellular location that might provide a
682 strong influence on the cell's spiking output (Figure 9). Light microscopy showed a
683 similar positioning of feedforward synapses near to the axon for the terminals of
684 MBON- γ 1pedc> α/β on MBON- β '2mp (Perisse et al., 2016) an MBON from
685 compartments at the tip of the horizontal lobe. The MBON- β 1> α and MBON-
686 γ 1pedc> α/β feedforward neurons also make synapses onto each other, but in an
687 asymmetric manner: MBON- β 1> α is nearly 4 times more likely to make synapses
688 onto MBON- γ 1pedc> α/β than *vice versa* in the α 2 and α 3 compartments (Figures 4F
689 and 9D; Table 5; we do not know the pattern of connections of these two neurons in
690 the α 1 compartment because, as explained above, we were unable to identify
691 MBON- γ 1pedc> α/β in this compartment.). Although the number of these axo-axonic
692 synapses is low, they may play a significant role in the interaction of different
693 memory modules, as they connect modules with different valence, and synaptic
694 input directly to an axon may have a large post-synaptic effect. While MBON- β 1> α ,
695 and to a lesser extent MBON- γ 1pedc> α/β , make some synapses onto KCs (Table 5)

696 there are on average only 0.37 of MBON- $\beta 1>\alpha$ to KC synapses per KC. Taken
697 together, our data suggest that the feedforward MBONs may have minimal impact
698 on the sensory representation provided by KCs in each compartment, but are likely
699 to modify the output conveyed by MBONs emerging from the α lobe.

700

701 **Discussion**

702
703 We have densely reconstructed the connectome of the α lobe of the adult Drosophila
704 MB, a region essential for long-term associative memory (Pascual and Preat, 2001,
705 Pai et al., 2013, Yu et al., 2006, Sejourne et al., 2011, Akalal et al., 2011, Blum et al.,
706 2009, Trannoy et al., 2011). The connections between the neurons we observed are
707 summarized in Figure 10. In each of the lobe's three compartments, parallel axonal
708 fibers of \sim 1,000 KCs project through the dendrites of a few MBONs and the terminal
709 arbors of a few DANs. Our results provide support for several aspects of the
710 generally accepted model for MB circuit function. First, we found that each KC
711 forms *en passant* synapses with multiple MBONs down the length of its axon,
712 making it possible for parallel processing across the different compartments of the
713 MB lobes. Secondly, with the assumption that released dopamine diffuses locally,
714 KC>MBON synapses would receive dopaminergic input close to the sites of vesicle
715 release, consistent with the prevailing hypothesis that plasticity occurs at the
716 presynaptic terminals of KCs (Heisenberg, 2003, McGuire et al., 2003, Zars et al.,
717 2000, Kim et al., 2007, Qin et al., 2012a). However, we also found several circuit
718 motifs that were not anticipated by previous work. For example, we found synaptic
719 connections from KCs to DANs, indicating that DANs get axo-axonal inputs within
720 the MB lobes themselves. A recent report provides evidence that these KC>DAN
721 synapses are functional (Cervantes-Sandoval et al., 2017). An even more
722 unexpected motif was the direct synaptic contacts from DAN to MBON we found in
723 every compartment. Our functional connectivity experiments confirmed that these
724 connections are monosynaptic, and showed that they give rise to a slow
725 depolarization in the MBON. Moreover, stimulating DANs in freely behaving flies
726 yields effects consistent with a net excitatory DAN>MBON connection. Finally, we
727 describe the synaptic connections of two feedforward MBONs, which have been
728 proposed to mediate the interaction of the various parallel memories within the MB
729 lobes, as well as two intrinsic MB neurons, APL and DPM.

730

731 Our work not only provides definitive evidence for, and quantitative detail about,
732 many previously observed circuit motifs, but also reveals several motifs not
733 anticipated by prior anatomical, behavioral or theoretical studies. These additional
734 circuit motifs provide new insights and raise new questions about the computations
735 carried out by the MB. We note that these same novel connections were also found
736 in a parallel study of the larval MB (Eichler et al., 2017 (in press)). Not only were the
737 same circuit motifs found in the larval MB and adult α lobe, but also the relative
738 prevalence of these connections was strikingly similar: DAN>MBON synapses were
739 4.5% the number of KC>MBON synapses in the adult α lobe and 3.4% in the larval
740 MB. KC>DAN synapses were 1.5 times as prevalent as DAN>KC synapses in the adult
741 α lobe, as compared with 1.1 in the larval MB. KCs make 48% of their synapses onto
742 other KCs in the adult α lobe and 45% in the larval upper vertical lobe
743 compartments. It is tempting to speculate that the conservation of the relative
744 abundances of these connections across developmental stages reflects important
745 functional constraints on the circuit.

746

747 **Parallel Processing in the Compartments of the MB**

748

749 A large body of work (reviewed in (Heisenberg, 2003, McGuire et al., 2005, Owald et
750 al., 2015)) supports the idea that individual KC>MBON synapses are the elemental
751 substrates of associative memory storage in the MB. The dominant hypothesis in the
752 field is that coincidence detection occurs within the presynaptic terminals of the
753 KCs. The Conditioned Stimulus (CS, for example an odor) evokes a spiking response
754 in a sparse subset of KCs, which in turn leads to Ca^{2+} influx. The Unconditioned
755 Stimulus (US, for example electric shock) activates dopaminergic inputs to the MB
756 lobes, where they likely activate G-protein coupled dopamine receptors on the KC
757 cell membrane. The coincidence of these two events is thought to be detected by the
758 Ca^{2+} sensitive, calmodulin-dependent adenylate cyclase *rutabaga*, which initiates a
759 cAMP signaling cascade that leads to the biochemical changes underlying synaptic
760 plasticity (Livingstone et al., 1984, Levin et al., 1992, Boto et al., 2014, Gervasi et al.,
761 2010, Tomchik and Davis, 2009).

762
763 The tiling of MBON and DAN projections down the length of the KC axons suggests
764 that each of these compartments serves as an independent module, with the
765 association of reinforcement with sensory input taking place in parallel across
766 several different modules. One important assumption in this model is that each KC
767 sends parallel input to each compartment by making synapses all the way down the
768 length of its axon. Light microscopic imaging established that the axons of
769 individual α/β KCs do indeed run through all three compartments of the α lobe (Aso
770 et al., 2014a). However, they also revealed that the axonal branching patterns differ
771 between KC classes (Aso et al., 2014a). For example, the axons of $\alpha/\beta p$ KCs branch
772 in $\alpha 2$ whereas those of $\alpha/\beta c$ and $\alpha/\beta s$ KCs do not, raising the question of how
773 extensive KC outputs are across the different compartments. Our dense EM
774 reconstruction allowed us to establish that in fact all α/β KCs form *en passant*
775 synapses on MBONs in each of the three α lobe compartments (Tables 2 and 3;
776 Videos 8-10).

777
778 In many cases these synapses were found at enlarged boutons that contained the
779 presynaptic machinery. However, output sites were also found on the smooth axons
780 of the $\alpha/\beta c$ KCs, which lack obvious bouton-like swellings. Only occasional, short
781 (generally $<5\mu m$) segments of KC axons where the axon became thinner than 300
782 nm in diameter lacked presynaptic sites. Of course, we do not know whether all
783 these synapses are functional. Our EM analysis showed that within each
784 compartment, every KC passing through a layer of the compartment that was
785 extensively innervated by an MBON made at least one synapse with that MBON.
786 Previous electrophysiological measurements of connectivity in the $\alpha 2$ compartment
787 indicated that only about 30% of KCs connect to MBON- $\alpha 2 sc$ (Hige et al., 2015b),
788 suggesting the possibility that the majority of KC>MBON synapses are functionally
789 silent, as they are in cerebellar cortex, where 98% of the parallel fiber-to-Purkinje
790 cell synapses are believed to be silent (Dean et al., 2010). However, we cannot rule
791 out a more trivial explanation: These measurements were made in the presence of

792 cholinergic antagonists that could have partially blocked synaptic events (Barnstedt
793 et al., 2016) and lead to an underestimate of total connectivity levels.

794

795 Our EM data revealed that the the number of synapses made by individual KCs was
796 well-described by a Poisson distribution, where each synapse connects with a
797 uniform, independent, and random probability to one of the KCs. Although the
798 predicted distributions strongly depend on the number of connections between two
799 celltypes, almost all KC connections to other cells obeyed Poisson statistics (Figure 4
800 – Figure Supplement 1). This was true of every KC in the $\alpha 1$ and $\alpha 3$ compartments,
801 where each MBON has compartment-filling dendrites. The $\alpha 2$ compartment is
802 somewhat unusual in that its MBONs innervate only subzones of the compartment
803 (Aso et al., 2014a). While light microscopy showed that MBON- $\alpha 2sc$ primarily
804 innervates the surface and core of the compartment, MBON- $\alpha 2sp$ was found to
805 project more to the surface and posterior. Our connectome results bore out these
806 observations from the light and electron microscopy, although EM reconstructions
807 also showed that these borders were not sharp, and these MBONs receive less
808 extensive and weaker connections outside these subzones (Table 3). Nevertheless,
809 within the primary area of innervation, it was again the case that every KC made
810 synapses with all MBONs along its axon. Thus each of the 949 α/β KCs can deliver
811 information to the MBONs in each of the three α lobe compartments.

812

813 A strictly feed-forward view of the circuit may miss important processing, however,
814 as earlier studies suggested, and our results re-emphasize. Firstly, gap junctions
815 between KCs have been reported (Liu et al., 2016). This opens up the possibility for
816 lateral propagation of signals across KCs, either biochemical or electrical. For
817 example, in mammalian systems, axo-axonal gap junction coupling can synchronize
818 firing between neurons (Traub et al., 2003, Schmitz et al., 2001). Secondly, chemical
819 synapses between KCs have been reported in the MB pedunculus in the locust
820 (Leitch and Laurent, 1996). Our reconstructions show that such KC>KC connections
821 are also present in the lobes, where they are surprisingly prevalent. In fact, the most

822 frequent outputs of the α/β s KCs are other α/β s KCs, assuming the morphologically
823 defined KC>KC connections are functional synapses.

824

825 A high percentage (55%) of these putative KC>KC synapses occur in rosette-like
826 structures where multiple KCs also converge on a single dendritic process of an
827 MBON (Figures 4A-C and 5A, B). These are relatively unusual structures, not
828 observed in EM reconstructions of the *Drosophila* visual system (Takemura et al.,
829 2008) and, indeed, we have no direct evidence that they are functional synapses. At
830 present we can only speculate on their role. As points of heavy convergence, they
831 might allow the effects of synapses from different KCs onto the same dendrite to act
832 synergistically. Activity of a single KC may spread to its neighbors within the
833 rosette, potentially generating a large compound synaptic release event onto the
834 MBON in the middle. Such a signal amplification mechanism may be important to
835 ensure that individual KCs can have a significant impact on MBON membrane
836 potential by recruiting their rosette partners. How the specificity of learning could
837 be maintained in this scenario is however unclear. Several basic questions will need
838 to be answered before we can begin to understand the functional significance of
839 these rosettes. For example, can a single KC in the rosette indeed activate its
840 neighbors? And how similar are the response properties of the different KCs that
841 contribute to one rosette?

842

843 In conclusion, the connectivity of the KCs that carry olfactory and other sensory
844 representations supports a model where parallel distributed memory processing
845 occurs in each compartment. However, several circuit motifs that seem designed to
846 spread and possibly amplify signals at the sites of KC output indicate that this circuit
847 is likely more complicated than a simple feed-forward view of the system suggests.

848

849 **Modulation by Dopamine**

850

851 Dopamine-induced plasticity of the KC>MBON synapse is thought to be central to
852 associative learning in this system (Owald et al., 2015, Hige et al., 2015a, Cohn et al.,

853 2015, Bouzaiane et al., 2015, Kim et al., 2007, Schwaerzel et al., 2003, Qin et al.,
854 2012b, Kaun et al., 2011, Rohwedder et al., 2016). Our reconstructions showed that
855 dopaminergic neurons make well-defined synaptic contacts within the α lobe, with
856 closely apposed post-synaptic membranes. This contrasts somewhat with
857 dopaminergic innervation in the mammalian system, where there is typically not
858 such close contact with a single clear post-synaptic partner, and volume
859 transmission is the predominant model for dopamine release (Gonon, 1997, Garris
860 et al., 1994). We do not know whether the direct and indirect dopaminergic release
861 sites have different functional consequences. Nevertheless, it seems likely that
862 some type of volume transmission happens in the mushroom body. First, we found
863 \sim 10 times more KC>MBON synapses than presynaptic sites of dopamine release in
864 the α lobe (Table 4; cf. Table 2), but previous work showed that learning-induced
865 plasticity depresses MBON responses so strongly that most inputs are likely affected
866 (Cohn et al., 2015, Hige et al., 2015b). Secondly, dopamine would need to diffuse
867 only \sim 2 μ m to reach every KC>MBON synapse within a compartment (Figure 4 –
868 figure supplement 2), but would also be sufficiently short range to prevent
869 significant spill-over of dopamine to neighboring compartments, ensuring that the
870 modularity of plasticity is maintained.

871
872 Functional connectivity measurements showed that stimulating the DANs elicits
873 large amplitude calcium signals from MBONs, similar to previous results (Sitaraman
874 et al., 2015). Our intracellular recordings revealed that this was a surprisingly
875 strong connection, sufficient to elicit spikes in the MBON (Figure 7). The response
876 persisted when we blocked both spiking and nicotinic transmission, to limit the
877 possibility that the DANs act through the KCs, which are cholinergic (Barnstedt et
878 al., 2016). Conversely, the response was strongly reduced by adding a dopamine
879 receptor antagonist. Taken together, these results indicate that the response is likely
880 a direct action of dopamine released by the DANs on the MBON, although we can not
881 formally rule out a more complex mechanism or a role for the transmitter contained
882 in the dense core vesicles we observed in the DANs. The depolarization exhibited
883 markedly slow dynamics, peaking >2 s after stimulation offset, and then decaying

884 over tens of seconds. Dopaminergic responses of similar amplitude and time course
885 have been reported in both mammalian systems (Zhou et al., 2009, Aosaki et al.,
886 1998) and in Aplysia, where it is mediated by cAMP-driven changes in a non-
887 selective cation conductance (Matsumoto et al., 1988).

888

889 **Implications for Memory Formation and Readout**

890

891 It is possible to induce memory formation in this circuit by pairing odor delivery
892 with artificial activation of DANs (Schroll et al., 2006, Claridge-Chang et al., 2009,
893 Aso et al., 2010, Aso et al., 2012, Yamagata et al., 2015, Liu et al., 2012, Burke et al.,
894 2012, Huetteroth et al., 2015, Perisse et al., 2013, Rohwedder et al., 2016).

895 Targeting this optogenetic training procedure to DANs that innervate different
896 compartments within the α lobe gives rise to memories with different valence,
897 induction threshold and persistence (Aso & Rubin, 2016). In the $\alpha 1$ compartment, a
898 single pairing for 1 min induces an appetitive memory that lasts for 1 day (Yamagata
899 et al., 2015, Ichinose et al., 2015, Huetteroth et al., 2015, Aso and Rubin, 2016). In
900 contrast, optogenetic training focused on the $\alpha 3$ compartment requires multiple 1
901 min pairings, repeated at spaced intervals, and induces an aversive memory that
902 lasts for 4 days (Aso and Rubin, 2016). Although it seems likely that the different
903 valences reflect the different projection sites of the MBONs for each of these
904 compartments, where the differences in induction threshold and memory
905 persistence might arise is less clear. There is no simple explanation for these
906 differences from the EM-level circuit structure, as the basic wiring motifs were very
907 similar in each compartment. Moreover, any explanation that invokes biochemical
908 differences in KC>MBON synapses would require crisp spatial localization of the
909 signaling pathway machinery that triggers plasticity, as exactly the same KCs
910 participate in memory formation in different compartments. However, our
911 observation that there are DAN>MBON synapses raises the possibility that
912 biochemical differences in the MBONs might contribute to these differences in
913 plasticity induction and maintenance. Indeed, RNAseq data from a set of four
914 different MBONs showed expression of dopamine receptors (Crocker et al., 2016).

915 An alternative possibility, suggested by our findings here, is that the cotransmitter
916 found in the dense core vesicles in the DANs is responsible for these differences.
917 The size of these vesicles differs between DANs innervating the different
918 compartments (Table 1). Thus these cells might release distinct co-transmitters, as
919 has been observed in mammalian brain (Stuber et al., 2010, Kim et al., 2015), which
920 could trigger different signaling cascades in either the KCs or the MBONs to
921 differentially modulate the induction and expression of plasticity across
922 compartments.

923

924 Models of MB function have generally considered the role for DANs to be confined to
925 relaying signals about punishment or reward to the MB. However in the
926 mammalian brain, DANs can dynamically change their responses to both US and CS
927 (Schultz, 1998). In this study, we found that the axonal terminals of the DANs
928 receive many inputs from KCs within the lobes. In other words, both MBONs, DANs
929 and even KCs receive extensive synaptic input from KCs in each compartment. If the
930 current model that plasticity is pre-synaptic proves to be correct, this suggests that
931 the responses of the DANs themselves would be subject to plasticity. If the synaptic
932 depression observed at KC>MBON synapses also acts at KC>DAN connections, odor-
933 evoked DAN responses would be diminished as a result of learning. This would
934 serve as a negative feedback loop, reducing the strength of plasticity on successive
935 training cycles with the same odor. Indeed, a gradually plateauing of the learning
936 curve is a common feature of memory formation in different systems (Rescorla and
937 Wagner, 1972, Bush and Mosteller, 1951), including olfactory conditioning in
938 Drosophila (Tully and Quinn, 1985).

939

940 One of the more surprising findings here was our observation that there are many
941 direct DAN>MBON synaptic connections. Moreover, our functional connectivity
942 measures indicate that these were relatively strong excitatory inputs. The
943 excitatory sign of the DAN>MBON connection is also consistent with the behavioral
944 effects of DAN activation we observed (Figure 8). What role these DAN>MBON
945 connections play in overall circuit function is an important question for future work.

946 There are two general possibilities that we feel are interesting to consider.
947 Dopaminergic modulation has been proposed to play a general role in routing of
948 information through the MB to different downstream neurons (Cohn et al., 2015,
949 Lewis et al., 2015, Perisse et al., 2016). Although changes in KC>MBON strength
950 contribute to this process (Cohn et al., 2015), our results here suggest that such
951 state changes could also potentially be conveyed to the MBONs directly from the
952 DANs. State-dependent changes in DAN activity have indeed been observed with
953 calcium imaging (Cohn et al., 2015, Musso et al., 2015, Berry et al., 2015, Perisse et
954 al., 2016, Krashes et al., 2009). The slow synaptic dynamics we observed in the
955 DAN>MBON connection in MBON- α 1 (Figure 7) suggest the possibility that small
956 changes in DAN firing might be capable of producing sustained changes in MBON
957 membrane potential reflecting the current internal state of the animal.

958

959 A second possibility, suggested from the framework of reinforcement learning
960 established in vertebrates (Zhang et al., 2009), is related to motivation and the
961 comparison of expected versus actual reward. In *Drosophila*, prior work on odor-
962 sugar conditioning in larvae provided evidence that flies form a comparison
963 between the current state of reward and the reward expected from the conditioned
964 cue (Schleyer et al., 2011). This work showed that animals behaviorally express
965 memories only when the expected reward intensity is higher than the currently
966 available reward (Schleyer et al., 2011, Schleyer et al., 2015). This is similar to the
967 results we presented here; just as the presence of reward diminished memory
968 expression in the larvae, stimulating the DANs suppressed performance of animals
969 trained by the optogenetic conditioning (corresponding results were also obtained
970 in larvae M. Schleyer, B. Gerber, L. Magdeburg, pers. comm.). The need to compare
971 current and expected reward could potentially explain why there is an opponent
972 relationship between the depression of KC>MBON synapses that drives associative
973 learning (Hige et al., 2015a, Cohn et al., 2015, Owald et al., 2015, Sejourne et al.,
974 2011, Bouzaiane et al., 2015) and the excitatory effects of the DAN>MBON
975 connection. If depression dominates, the association drives behavior, but this can
976 be overridden by sufficient levels of DAN activity. In this respect, it is noteworthy

977 that DANs appear to be able to act directly on the MBON, without participation of
978 the KCs. Overall this comparison could ensure that learned behavior is motivated
979 not strictly by the expectation of reward, but rather the expected increase in reward,
980 assessed at the moment of testing (Schleyer et al., 2015, Schleyer et al., 2011).

981

982 **Feedforward Coordination of Parallel Memory Modules**

983

984 The organization of the MB into a set of compartments arranged in series along the
985 KC axons is well suited for simultaneously storing multiple independent memories
986 of a given sensory stimulus (Das et al., 2014, Kaun et al., 2011, Aso and Rubin, 2016).
987 However, there must be some means by which these modules interact with one
988 another to ensure coordinated, coherent expression of memory. Feedforward
989 connections that link different compartments, first discovered by light microscopic
990 anatomy (Tanaka et al., 2008, Aso and Rubin, 2016), have recently been shown to be
991 important for mediating such interactions. In particular, MBON- $\gamma 1pedc>\alpha/\beta$ is an
992 inhibitory neuron that connects aversive and appetitive learning compartments; it
993 ensures that the circuit can readily toggle between different behavioral outputs
994 (Perisse et al., 2016, Aso and Rubin, 2016).

995

996 Our EM reconstructions included both MBON- $\gamma 1pedc>\alpha/\beta$ and MBON- $\beta 1>\alpha$, two
997 feedforward neurons which project from their respective compartments to widely
998 innervate other parts of the MB. Memories stored in the α lobe compartments are
999 long-term and relatively inflexible, whereas the short-term memories formed in $\beta 1$
1000 and $\gamma 1pedc$ are readily updated by recent experiences. The feedforward
1001 connections are thought to enable the short-term memories in $\beta 1$ and $\gamma 1pedc$ to
1002 temporarily mask expression of the stable memories stored in the α lobe. Indeed
1003 training an animal with either a multi-component aversive/appetitive food stimulus
1004 (Das et al., 2014), or by simultaneous optogenetic activation of a composite set of
1005 DANs covering both appetitive and aversive compartments (Aso and Rubin, 2016)
1006 results in a compound memory that is initially aversive and later transitions to
1007 appetitive. Our connectome results show that the primary synaptic targets of these

1008 feedforward neurons are the MBONs in the downstream compartment (Table 5). By
1009 contrast, we observed relatively few connections onto KCs. Overall this suggests
1010 that the feedforward connections can strongly influence the output from a
1011 compartment, but likely have little impact on the sensory information delivered to
1012 each compartment from the KCs. This is consistent with observations that MBON-
1013 $\gamma 1pedc>\alpha/\beta$ strongly modulates activity of glutamatergic neurons at the tip of the
1014 horizontal lobe, but not their dendritic responses (Perisse et al., 2016). Targeting
1015 these feedforward connections to the MBON may ensure that conflicting memories
1016 can form simultaneously in response to a complex sensory input, but with the
1017 behavioral manifestation of those memories capable of undergoing a crisp switch.
1018

1019 **Concluding Remarks**

1020

1021 We provide synapse level anatomical information on neuronal circuits involved in
1022 learning and memory in *Drosophila*. The comprehensive nature of this dataset
1023 should enable modeling studies not previously possible and suggests many
1024 experiments to explore the physiological and behavioral significance of the circuit
1025 motifs we observed. That many of these motifs were not anticipated by over thirty
1026 years of extensive anatomical, experimental and theoretical studies on the role of
1027 the insect MB argues strongly for the value of electron microscopic connectomic
1028 studies.

1029

1030 A dense (complete) reconstruction of neurons and synapses is resource intensive, so
1031 it is reasonable to ask if tracing a subset of cells or synapses could have yielded
1032 similar results with less effort. This is hard to answer in general, since there are
1033 many sparse tracing strategies, and each can be pursued to differing degrees of
1034 completeness. It is likely that most sparse tracing strategies would have discovered
1035 the new pathways reported here, as the connections are numerous and connect well
1036 known cell types. Conversely, the conclusions that all cell types in this circuit had
1037 been identified would have been more difficult to make with confidence and a rare
1038 cell type, such as the SIFamide neuron, might have been missed. Perhaps most

1039 importantly, statistical arguments, particularly those that require an accurate
1040 assessment of which cells are not connected, such as the absence of network
1041 structures such as rings or chains, would have been hard to make from sparse
1042 tracing. More generally, the model independent nature of dense tracing helps to
1043 discover any “unknown unknowns”, provides the strongest constraints on how
1044 neural circuits are constructed, and allows retrospective analysis of network
1045 properties not targeted during reconstruction.

1046

1047

1048 **Methods**

1049

1050 **Sample preparation**

1051

1052 The head of a 5-day old male progeny of a cross between a CantonS female and *w¹¹¹⁸*
1053 male was cut into 200 µm slices with a Leica VT1000 vibratome in 2.5 %
1054 glutaraldehyde, 2.5 % paraformaldehyde, 0.1 M cacodylate at pH 7.3. The resulting
1055 slices were allowed to fix for between 10 and 15 min and then transferred to 25 %
1056 aqueous bovine serum albumin for a few minutes before loading into a 220 µm deep
1057 specimen carrier and high-pressure frozen using a Wohlwend HPF Compact 01 high
1058 pressure freezing machine (Wohlwend GmbH). The samples were then freeze-
1059 substituted in a Leica EM AFS2 low temperature embedding system in 1% osmium
1060 tetroxide, 0.2 % uranyl acetate and 5 % water in 99% acetone with 1 % methanol,
1061 for 3 days (Takemura et al., 2013). The temperature was then raised to 21 °C,
1062 samples were rinsed in pure acetone, infiltrated, and embedded in Durcupan epoxy
1063 resin (Fluka). After a 48 h polymerization, the sample was previewed using 3D X-ray
1064 microscopy (Zeiss Xradia 510 Versa), oriented and then trimmed into a ~200 x 200
1065 x 200 µm tab centered around the mushroom body location for FIB-SEM imaging.

1066

1067 **Data acquisition**

1068

1069 The image data was collected using the methods described by (Xu et al., 2017) The
1070 trimmed sample was coated with 10 nm of gold and 100 nm of carbon. The
1071 mushroom body was oriented vertically with the α3 compartment at the top. Three
1072 dimensional isotropic structural data was acquired by focused ion-beam milling
1073 scanning electron microscopy, FIBSEM, with a Zeiss NVision40 instrument. A
1074 focused beam of 30 kV gallium atoms scanned across the top flat of the sample and
1075 ablated away 2 nm over a 180 x 180 µm area. A smaller region of roughly 40 x 40
1076 µm defined the imaging area of the scanning electron microscope. The sample was
1077 positively biased to 400 volts and scanned in x and y with 8 nm pixels, at 3

1078 nanoamperes and 1.1 KeV landing energy. The signal was acquired at 1.25 MHz per
1079 pixel using an in-column detector of the back-scattered electrons. About 60,000
1080 such ablation and imaging cycles over a 5-week period formed the raw data set.
1081 After registration of the images using affine transformations, sequential sets of four
1082 2 nm (in z) images were averaged together to form a main data set with 8 nm
1083 isotropic voxels.

1084
1085 Subsequent imaging for the higher resolution (~4x4x4 nm voxels) data was taken
1086 on a small volume of a different mushroom body sample prepared in the same way,
1087 but imaged at 0.2 nanoamperes, 700 volts landing energy and 200 KHz sampling
1088 rate. Such data complemented the whole MB data to show better detail of typical
1089 synaptic motifs.

1090

1091 **Data Processing**

1092

1093 We defined a region of interest (ROI) containing the α lobe of the mushroom body,
1094 using the distinct glia surrounding the α lobe neuropil and its distinctive
1095 morphology.

1096

1097 Within the ROI, we first automatically generated presynaptic locations. A Deep and
1098 Wide Multiscale Recursive (DAWMR) network (Huang, 2013) was trained on a
1099 subset of manually defined presynaptic densities. The final T-bar point predictions
1100 from the voxel-wise output of the DAWMR network were obtained by spatially
1101 smoothing the voxel-wise predictions, selecting the voxels with highest confidence,
1102 and applying non-maxima suppression (Huang, 2014). Since manual verification
1103 followed, centered at the selected points, the parameters were tuned to favor
1104 completeness, achieving roughly 75% accuracy at 90% recall.

1105

1106 Next, the FIBSEM imaged volume, starting with the ROI, was segmented
1107 automatically with an algorithm similar to that described in (Parag et al., 2015). The
1108 ROI was divided into $\sim 70 \mu\text{m}^3$ subvolumes with some overlap between them. For

1109 each subvolume, an initial oversegmentation was generated by the standard
1110 watershed method from the outputs of a voxel predictor. The oversegmented
1111 regions were refined by a supervoxel agglomeration technique. The particular
1112 staining method adopted for this dataset resulted in artifacts such as occasional
1113 breaks and holes on the cell membranes. We developed a “conservative” training
1114 strategy for the voxel predictors that was biased towards minimizing false merges
1115 between two neurons. The supervoxel boundary classifier required for the
1116 agglomeration is trained using the small sample learning algorithm of (Parag et al.,
1117 2014) that eliminates the necessity of exhaustively labeled ground truth. The
1118 overlapping subvolumes were stitched together using the strategies outlined in
1119 (Plaza, 2016b). After the ROI was proofread (described below), segmentation was
1120 generated for the surrounding region of the α lobe to enable sparse tracing.

1121
1122 A manual verification and correction step (proofreading) followed the automatic
1123 synapse detection and segmentation. The synapses for the α lobe were annotated
1124 using the protocol in (Plaza et al., 2014). The automatic prediction of presynaptic
1125 sites was tuned for high recall (as described above), and the sites were validated by
1126 proofreaders. After this, a different proofreader re-examined each of these
1127 presynaptic annotations and further annotated the postsynaptic cell partners. We
1128 used a special tag to denote convergent synapses.

1129
1130 After the completion of synapse annotation, we divided the volume into small
1131 overlapping subvolumes and applied focused proofreading (Plaza, 2016a) to revise
1132 the initial segmentation, which was tuned to be over-segmented. This protocol was
1133 executed in Raveler (<https://openwiki.janelia.org/wiki/display/flyem/Raveler>) and
1134 entails a series of yes/no merge decisions for adjacent segments where the
1135 segmentation classifier was uncertain. After focused proofreading, the proofread
1136 subvolume results were integrated into the complete dataset. At this point, there
1137 are many unassigned synapses because those synaptic annotations are on small
1138 fragmented bodies, which we call synaptic orphans. To make the connectome as
1139 complete as possible, we reviewed and, where possible to do so with high

1140 confidence, assigned the orphan fragments to a larger reconstructed neuron. We
1141 used NeuTu-EM (https://github.com/janelia-flyem/NeuTu/tree/flyem_release)
1142 (Zhao et al., 2017) to proofread the segmentation on the large dataset, and DVID
1143 (<https://github.com/janelia-flyem/dvid>) (Katz & Plaza, 2017) to manage the data
1144 and provenance of these changes. Select neurons were sparsely traced outside of
1145 the densely reconstructed α lobe using NeuTu-EM.

1146

1147 **Statistical methods**

1148

1149 When testing if the observed connectivity is compatible with a Poisson distribution
1150 we compute such a distribution with the same mean and total connectivity. Using
1151 all entries with expected value at least 0.5, we compute a χ^2 value and from this an
1152 estimate of p. When testing whether two connectivities are independent we use
1153 Fischer's exact test. To test whether two distributions are drawn from the same
1154 underlying distribution, we use the Kolmogorov-Smirnov test. When finding
1155 correlation between two synapse strength vectors, we use Pearson's correlation
1156 coefficient.

1157

1158 **Calcium Imaging**

1159

1160 Flies were reared at 25°C on retinal supplemented (0.2mM) cornmeal medium that was
1161 shielded from light. All experiments were performed on female flies, 2-4 days after
1162 eclosion with the genotype: 10xUAS-Syn21-Chrimson-tdTomato 3.1 in attP18,
1163 13xLexAop2-IVS-Syn21-opGCaMP6s in su(Hw)attP8; R58E02-p65ADZp in
1164 VK00027/+; R32D11-ZpGAL4DBD in attP2; 52G04-LexA flies (opGCaMP6s and
1165 Chrimson-tdTomato are codon optimized reagents that were the gift of Barrett Pfeiffer
1166 and David Anderson). Brains were dissected in a saline bath (103mM NaCl, 3mM KCl,
1167 2mM CaCl₂, 4mM MgCl₂, 26mM NaHCO₃, 1mM NaH₂PO₄, 8mM trehalose, 10mM
1168 glucose, 5mM TES, bubbled with 95% O₂ / 5% CO₂). After dissection, the brain was
1169 positioned anterior side up on a coverslip in a Sylgard dish submerged in 3ml saline at
1170 20°C.

1171
1172 The sample was imaged with a resonant scanning 2-photon microscope with near-
1173 infrared excitation (920nm, Spectra-Physics, INSIGHT DS DUAL) and a 25x objective
1174 (Nikon MRD77225 25XW). The microscope was controlled by using ScanImage 2015.v3
1175 (Vidrio Technologies). Images were acquired with 141 μm x 141 μm field of view at
1176 512x512 pixel resolution, approximately 9 Hz frame rate after averaging 5 frames. The
1177 excitation power for calcium imaging measurement was 12mW.

1178
1179 For the photostimulation, the light-gated ion channel Chrimson was activated with a 660-
1180 nm LED (M660L3 Thorlabs) coupled to a digital micromirror device (Texas Instruments
1181 DLPC300 Light Crafter) and combined with the imaging light path using a FF757-DiO1
1182 dichroic (Semrock). On the emission side, the primary dichroic was Di02-R635
1183 (Semrock), the detection arm dichroic was 565DCXR (Chroma), and the emission filters
1184 were FF03-525/50 and FF01-625/90 (Semrock). Photostimulation light was delivered in a
1185 pulse train that consisted of three 100 msec pulses with a 60 sec inter-pulse interval. The
1186 light intensity was 0.24 mW/mm², as measured using Thorlabs S170C power sensor.

1187
1188 Calcium responses were recorded as changes in fluorescence in a manually defined
1189 region of interest in the $\alpha 1$ compartment. Tetrodotoxin (American Radiolabeled
1190 Chemicals) and mecamylamine (Sigma) were then applied as 15x stock into the bath to
1191 reach 1 μM and 250 μM final concentration, and brains incubated for 4 minutes to allow
1192 permeation before recording another round of responses. The second of the three pulses
1193 in the train were plotted as mean \pm SEM without normalization.

1194
1195 **Electrophysiology**

1196
1197 *In vivo* whole-cell recordings and photostimulation were performed as previously
1198 described (Hige et al., 2015). The pipette solution contained (in mM): L-potassium
1199 aspartate, 125; HEPES, 10; EGTA, 1.1; CaCl₂, 0.1; Mg-ATP, 4; Na-GTP, 0.5; biocytin
1200 hydrazide, 13; with pH adjusted to 7.3 with KOH (265 mOsm). The preparation was
1201 continuously perfused with saline containing (in mM): NaCl, 103; KCl, 3; CaCl₂, 1.5;

1202 MgCl₂, 4; NaHCO₃, 26; N-tris(hydroxymethyl) methyl-2-aminoethane-sulfonic acid, 5;
1203 NaH₂PO₄, 1; trehalose, 10; glucose, 10 (pH 7.3 when bubbled with 95% O₂ and 5% CO₂,
1204 275 mOsm). For photostimulation, we used a single red LED with peak wavelength of
1205 627 nm (LXM2-PD01-0050; Philips) to illuminate the brain through a 60X water-
1206 immersion objective (LUMPlanFl/IR; Olympus) at an intensity of 1.1 mW/mm². Stimuli
1207 were 2 msec in duration, delivered every 75 sec. After recording 3-5 trials, tetrodotoxin
1208 and mecamylamine were applied by perfusion into the bath at final concentrations of 1
1209 μM and 250 μM respectively, as in the imaging experiments. We used female flies of the
1210 same genotype and raised in the same way as those used for calcium imaging
1211 experiments, targeting the cells using baseline GCaMP signal. We obtained qualitatively
1212 similar results (data not shown) in recordings using Chrimson R to activate the DANs
1213 and GFP to label the MBON in flies with the genotype 10xUAS-ChrimsonR-mVenus
1214 (attP18)/+; R71C03-LexAp65 in attP40/ LexAop-GFP in su(Hw)attP5; MB043C/+ . We
1215 tested the role of dopamine receptors by recording responses to DAN photostimulation in
1216 the presence of tetrodotoxin and mecamylamine and then perfusing the antagonist SCH
1217 23390 (100 μ M final concentration) into the bath. For these experiments, flies were of
1218 genotype: 10xUAS-ChrimsonR-mVenus in attP18/+; R71C03-LexAp65 in attP40/
1219 LexAop-GFP (attP5); MB043C/+ . To measure the transmission between KCs and the
1220 MBON, we expressed ChrimsonR in all α/β KCs using the Split-GAL4 line, MB008D
1221 (R13F02-p65ADZp in VK00027, R44E04-ZpGAL4DBD in su(Hw)attP2). The genotype
1222 of the flies was 10xUAS-ChrimsonR-mVenus in attP18/+; R71C03-LexAp65 in
1223 attP40/LexAop-GFP in su(Hw)attP5; MB008D/+.

1224

1225

1226 **Behavioral experiments**

1227

1228 Olfactory learning assays were performed using the four-field optogenetic olfactory
1229 arena as previously described (Aso and Rubin 2016) using thirty 1 s pulses of red
1230 LEDs for activation (627 nm peak and 34.9 μW/mm²). For testing the conditioned
1231 response in the presence of DAN activation thirty times of 1 s pulses of red light ON
1232 and 1s OFF were delivered spread over the 60 s test period. Crosses of split-GAL4

1233 lines for DANs, MB043C and MB630B (Aso et al., 2014a; Aso and Rubin 2016), and
1234 20xUAS-CsChrimson-mVenus in attP18 (Klapoetke et al., 2014) were kept on
1235 standard cornmeal food supplemented with retinal (0.2 mM all-trans-retinal prior to
1236 eclosion and then 0.4 mM) at 22 °C at 60% relative humidity in the dark. Female
1237 flies were sorted on cold plates at least 1 d prior to the experiments and 4–10 d old
1238 flies were used for experiments. Groups of approximately 20 females were trained
1239 and tested at 25°C at 50% relative humidity in a dark chamber. The odors were
1240 diluted in paraffin oil (Sigma–Aldrich): 3-octanol (OCT; 1:1000; Merck) and 4-
1241 methylcyclohexanol (MCH; 1:1000; Sigma–Aldrich). For appetitive memory assays
1242 using MB043C, flies were starved for 48 h on 1% agar. Videography was performed
1243 at 30 frames per second and analyzed using Fiji (Schindelin et al., 2012). Statistical
1244 comparisons were performed using Prism (Graphpad Inc, La Jolla, CA 92037).

1245

1246 **Videos:**

1247

1248 Video 1: A portion of the dataset that was used for connectome reconstruction
1249 shown at down-sampled resolution. Approximately 9,600 sequential x-y imaging
1250 planes are shown covering a 35 x 35 x 77 μm region of the complete image volume
1251 (40 x 50 x 120 μm). The original voxel size was 8 x 8 x 8 nm; the video has been
1252 down sampled by a factor of eight, making the voxel size shown 64 x 64 x 64 nm.
1253 The video progresses from top of the vertical lobe, which is ensheathed in glia,
1254 through the α_3 and α_2 compartments as indicated by the black bracket in Figure 1B.

1255

1256 Video 2: A portion of the data set that was used for connectome reconstruction
1257 shown at the resolution at which the data was acquired, 8 x 8 x 8 nm voxels. The
1258 region shown corresponds to the portion of the α_3 compartment indicated by the
1259 white box in Figure 1B.

1260

1261 Video 3: All KCs in the α lobe, except outer-core ($\alpha/\beta\text{c(o)}$). A total of 259 $\alpha/\beta\text{c(i)}$,
1262 480 $\alpha/\beta\text{s}$, and 78 $\alpha/\beta\text{p}$ KCs are shown colored in ivory, orange and yellow,
1263 respectively.

1264

1265 Video 4: Tiling of the MBONs and DANs in the α lobe. Neurites of MBONs and DANs
1266 are confined to a single compartment where they are intermingled. Two MBON- α_3 ,
1267 two PPL1- α_3 and the one MBON- $\alpha_2\text{sc}$ are shown in sequence.

1268

1269 Video 5: PAM- α_1 DANs. Individual morphologies of 16 PAM- α_1 neurons are
1270 displayed in sequence showing how the terminals of these cells collectively fill the
1271 compartment.

1272

1273 Video 6: Distribution of synaptic inputs onto MBON- α_3 arbor. MBONs in each
1274 compartment receives thousands of synaptic inputs from KCs as well as DANs and
1275 feedforward MBONs.

1276
1277 Video 7: Distribution of sites of single input and convergent synapses. Synaptic
1278 inputs onto an MBON arbor as single synapses are uniformly distributed over the
1279 MBON dendrites and the inputs of convergent/rosette synapses are found much
1280 more frequently.
1281
1282 Video 8: Inner core KCs ($\alpha/\beta c(i)$). Five cells are displayed first with presynaptic
1283 locations indicated by magenta puncta. All other reconstructed core KCs are then
1284 added.
1285
1286 Video 9: Surface KCs ($\alpha/\beta s$). Five cells are displayed first with presynaptic locations
1287 indicated by magenta puncta. All other reconstructed surface KCs are then added.
1288
1289 Video 10: Posterior KCs ($\alpha/\beta p$). Five cells are displayed first with presynaptic
1290 locations indicated by magenta puncta. All other reconstructed posterior KCs are
1291 then added.
1292
1293 Video 11: A few APL branches are randomly picked and separated from the main
1294 body to show their morphological features. APL branches are first shown
1295 individually and then in combination.
1296
1297
1298
1299 **Figures:**
1300
1301 **Figure 1:** Diagram of the α lobe of the mushroom body.
1302 (A) An image of the adult brain showing the antennal lobes (AL), the mushroom
1303 bodies (MB) and an example of one of the ~50 types of projection neurons (PN) that
1304 carries olfactory information from the AL to the MB calyx and the lateral horn (LH).
1305 See Aso et al. (2014a) for more detail. The approximate position of the ~40 x 50 x
1306 120 μm volume imaged by FIBSEM is indicated by the red dashed lines. (B)
1307 Magnified view of the α/β lobes showing the imaged volume. The α/β neurons
1308 bifurcate in the $\alpha 1$ compartment and project to the α and β lobes. The white box

1309 indicates the portion of the α 3 compartment shown in Video 2. (C) Simplified
1310 diagram of the circuit organization in the α lobe. The projection patterns of the
1311 axons of dopaminergic neurons (DANs) and the dendrites of the MB output neurons
1312 (MBONs) onto the parallel axonal fibers of Kenyon cells define three compartmental
1313 units in the α lobe. The DANs (green) and MBONs with dendrites in the α 1, α 2 and
1314 α 3 compartments (purple), known from previous light microscopic studies (see Aso
1315 et al. 2014a for more detail), are indicated. Arrows indicate the main presynaptic
1316 sites of each of the extrinsic neuron types. The names of neurons (shown in the
1317 rectangles with rounded corners) are color-coded to reflect their main
1318 neurotransmitter: black, dopamine; orange, acetylcholine; green, glutamate; blue,
1319 GABA. In addition to MBONs with dendrites in the α lobe, all three compartments
1320 receive projections from the GABAergic MBON- γ 1pedc> α/β (dark blue) and the
1321 glutamatergic MBON- β 1> α feedforward neurons (magenta), whose dendrites lie in
1322 other MB lobes.
1323

1324

1325 **Figure 2:** Reconstructions of cells present in the α lobe.
1326 In panels (A)-(M) and (O), the upper image shows EM reconstructions generated as
1327 part of this study and the lower image shows the same cell type, segmented from
1328 previously acquired light microscopic images (Aso et al. 2014a). The EM
1329 reconstructions are limited to that portion of the neurons found in the α lobe, while
1330 the light images show the portion of each neuron found in the entire MB. (A) A total
1331 of 949 α/β Kenyon cells (KCs) were traced: 871 surface and core KCs (khaki); 78
1332 posterior KCs (yellow). (B) The glutamatergic feedforward neuron, MBON- β 1> α ,
1333 arborizes in all three compartments of the α lobe. (C) The arborizations of the ipsi-
1334 and contralateral MBON- γ 1pedc> α/β , GABAergic feedforward neurons, are shown
1335 separately in the upper panel. (D) The GABAergic APL neuron arborizes throughout
1336 the MB lobes and calyx. (E) The DPM neuron arborizes throughout the MB lobes.
1337 (F) The SIFamide neuron arborizes very widely, extending throughout the brain;
1338 only the α lobe arborizations are shown. Panels (G)-(M) and (O) show compartment
1339 specific MB output neurons (MBONs) and dopaminergic neurons (DANs). The α 3
1340 compartment has the axonal terminals of two DANs, PPL1- α 3 (G), and the dendrites
1341 of two MBONs, MBON- α 3 (H). The α 2 compartment has two DANs, PPL1- α' 2 α 2 (I),
1342 and four MBONs: a single MBON-a2sc (J); two MBON- α 2p3p (K); and one newly
1343 found MBON, MBON- α 2sp (L). The α 1 compartment has 16 DANs, PAM- α 1 (M in
1344 aggregate and N as individual cells), and two MBONs, MBON- α 1 (O).

1345

1346

1347 **Figure 3:** Profiles of reconstructed neurons in an EM cross section at the depth of
1348 α 3.
1349 (A) All the reconstructed neurons that have neurites at this depth are color-labeled
1350 using the same color scheme as in Figure 2. (B)-(E) Subsets of cell types are shown
1351 separately: (B) dendrites of the two MBON- α 3 cells; (C) axonal projections of the
1352 two PPL1- α 3 DANs; (D) axonal feedforward projects of MBON- β 1> α and MBON-

1353 $\gamma 1pedc>\alpha/\beta$, of which only a few small profiles can be seen in a single section; and
1354 (E) APL, DPM and SIFamide neurons. Scale bars: 5 μ m.

1355

1356

1357 **Figure 4:** Examples of synaptic motifs in the α lobe.

1358 (A) Five KCs are shown, converging once in the α lobe to form a rosette synapse
1359 (arrow). (B,C) EM cross section of the rosette synapse formed by these five KCs.
1360 Each KC is colored in (B) with the same color as the corresponding reconstructed
1361 cell in (A). (C) The same EM image as (B) with a dendrite of an MBON (asterisk).
1362 Presynaptic specializations of the KCs are indicated by red arrowheads at which KCs
1363 contact with both the MBON and neighboring KC. (D) A PAM- $\alpha 1$ dopaminergic
1364 neuron synapses onto MBON- $\alpha 1$ and KCs in the $\alpha 1$ compartment; the red arrowhead
1365 marks the presynaptic specialization in PAM- $\alpha 1$. (E) Two KCs synapse onto a PPL1-
1366 $\alpha 3$ dopaminergic neuron. An adjacent MBON (asterisk) also appears to receive
1367 input from one of these KCs. (F) The MBON- $\beta 1>\alpha$ feedforward neuron makes an
1368 axon-axonal synapse onto the MBON- $\gamma 1pedc>\alpha/\beta$ feedforward neuron, as well as a
1369 synapse onto MBON- $\alpha 3$ dendrites, in the $\alpha 3$ compartment; the presynaptic
1370 specialization in MBON- $\beta 1>\alpha$ is marked by a red arrowhead. (G) The MBON-
1371 $\gamma 1pedc>\alpha/\beta$ feedforward neuron synapses onto MBON- $\alpha 3$ dendrites; the presynaptic
1372 specialization in MBON- $\gamma 1pedc>\alpha/\beta$ is marked by a red arrowhead. Scale bar: 500 nm,
1373 applies to panels (B)-(G).

1374

1375

1376 **Figure 4 – figure supplement 1:** Poisson distribution of KC output connectivity.

1377 (A) The number of synapses made by individual KCs onto each of the two pairs of
1378 output neurons from the $\alpha 3$ and $\alpha 1$ compartments (KC- α/β s > MBON- $\alpha 3$ and KC-
1379 α/β p > MBON- $\alpha 1$). Points represent experimentally observed synapse numbers,
1380 bars represent SD of Poisson fits to the experimental distributions. Both MBONs
1381 within each compartment show similar distributions, all of which show Poisson
1382 statistics. (B) Poisson statistics of KC connectivity. Each entry is a p -value
1383 expressing the likelihood that the observed distribution of synapse numbers is
1384 compatible with a Poisson distribution of the same mean. Connections where KCs
1385 were pre-synaptic (left) and post-synaptic (right) were evaluated
1386 independently. Green entries are statistically indistinguishable from Poisson ($p >$
1387 0.05), magenta entries are more than 3 sigma different ($p < 0.003$), and yellow
1388 entries are intermediate. Most distributions were not significantly different from
1389 Poisson. (C) Distributions of synapse numbers for connection types whose
1390 distribution showed the strongest deviation from Poisson in (B). Our
1391 reconstructions showed that the KC- α/β c(i) > DPM connections deviate from
1392 Poisson likely because DPM processes do not strongly innervate the very core of the
1393 α -lobe. The other examples deviate because a few cells are connected with high
1394 numbers of synapses, which a Poisson distribution predicts is very unlikely.

1395

1396

1397 **Figure 4 – figure supplement 2:** Synapse specificity with volume transmission of
1398 dopamine. Plots show the fraction of KC>MBON synapses with a dopaminergic
1399 output synapse within the indicated range. Blue lines show cumulative fraction with
1400 dopaminergic synapse from the same compartment, red line represents cumulative
1401 fraction with a DAN output in an adjacent compartment. These plots indicate that
1402 there is a wide tolerance for volume transmission in every compartment; essentially
1403 all KC>MBON synapses are within a 2 micron diffusion range of a DAN synapse from
1404 the same compartment, yet much larger diffusion distances would be necessary for
1405 DAN outputs in other compartments to reach them.

1406

1407

1408 **Figure 5:** Images from the higher resolution dataset and examples of the
1409 distribution of synapses on a KC. (A) A triangular motif of KC<>KC>MBON synapses.
1410 Presynaptic densities in two adjacent KCs (arrowheads) contact to an MBON
1411 (asterisk); the KCs also appear to make reciprocal contacts. (B) A rosette synapse
1412 formed by a postsynaptic MBON (asterisk) surrounded by five KCs. (C) The α_3 and
1413 α_2 portion of a core KC that has a total of 63 presynaptic sites in the α lobe (red
1414 puncta) is shown. This KC makes 49 synapses onto MBONs; the remaining 14
1415 synapses are onto other cell types such as APL and DPM. (D) Sites where the same
1416 KC as in (C) is postsynaptic (black puncta) are also shown: Of the 114 inputs this KC
1417 receives in the α lobe, 94 come from 65 other core KCs; 13 from 11 different surface
1418 KCs; 4 from DANs (3 times in α_3 and once in α_1); and 3 from APL. Note that because
1419 multiple synapses can occur in close proximity the number of distinct puncta visible
1420 is smaller than the number of synapses and that red and black puncta are often co-
1421 localized, indicating the KC is pre- and postsynaptic at the same site on its axon. (E)
1422 We found three kinds of synaptic vesicles in neurons in the α lobe: rounded clear
1423 vesicles (white arrowheads), small-rounded dense-core vesicles (yellow
1424 arrowheads), and larger dense-core vesicles (double-arrowheads). Scale bars: 500
1425 nm in (A, B, E).

1426

1427

1428 **Figure 6:** Connectivity profiles of the different neuron classes in the lobes.
1429 (A) Input profiles of different cell types within each α lobe compartment. All cells
1430 within a cell type are combined, so for example DAN inputs in the α_1 compartment
1431 represent the inputs to all 16 PAM- α_1 neurons, while in α_2 it is the two PPL1- $\alpha'_2\alpha_2$
1432 neurons and in α_3 it is the two PPL1- α_3 cells. Bar heights indicate the total number
1433 of input synapses from the different sources, with KC-c(i) indicating α/β KCs from
1434 the inner core, and KC-c(o) the outer core. The feedforward MBONs were omitted
1435 from these profiles; see Table 5 for the distribution of their synaptic outputs. The
1436 input profiles of the DANs and particularly the MBONs are quite distinct in each
1437 compartment. By comparison, APL and DPM input profiles are very similar across
1438 compartments, suggesting they uniformly pool input from multiple compartments.
1439 (B) Output profiles. Note the overall similarity of output connectivity of APL and
1440 DPM across all three compartments – aside from the numerous DPM>MBON
1441 connections observed in α_1 . Again, this contrasts with the output profiles of the
1442 DANs, which are quite different in each compartment. Note that we did not find any

1443 output sites of MBONs, except for ones providing feedforward input from other
1444 compartments, indicating that MBONs are strictly dendritic inside the lobe (C)
1445 Primary connectivity motifs observed. Thick arrows indicate connections composed
1446 of >200 synapses, thin arrows >50 synapses in at least two compartments, and
1447 connections with fewer than 50 synapses are not represented in this schematic (but
1448 see Figure 6 – figure supplement 1). Red arrows indicate synaptic connections
1449 newly identified in this study; similar connections were also seen in parallel
1450 connectomics studies of the larval MB (Eichler et al., 2017 (in press)).
1451
1452

1453 **Figure 6 – figure supplement 1:** Connectivity matrix of cell types in the α lobe.
1454 Numbers of synapses detected between different circuit elements corresponding to
1455 the graphical display in Figure 6. Left column indicates the compartment where the
1456 connections were observed, and the next column shows cell types presynaptic to the
1457 cell types shown in the top row. In α 3, PPL refers specifically to two PPL1-
1458 α 3neurons, in α 2 it is the two PPL1- α' 2 α 2 cells and in α 1 it is 16 PAM- α 1 neurons.
1459 The MBONs do not make any output synapses within the lobes and so are omitted
1460 from the rows of the matrix. Red shading indicates synaptic connections newly
1461 identified in this study.
1462
1463

1464 **Figure 7:** Functional connectivity between DAN and MBON in the α 1 compartment.
1465 (A) Experimental schematic. Chrimson-expressing PAM- α 1 DANs were
1466 photostimulated and MBON- α 1 responses measured either with the calcium sensor
1467 GCaMP6s or with whole cell recordings targeted via GCaMP fluorescence. (B) Calcium
1468 response of MBON to DAN photostimulation. Dark blue trace shows fluorescence
1469 values taken from the dendritic region of the MBON, with photostimulation (100 msec)
1470 demarcated by the red bar (mean + SEM of recordings from n = 7 different flies). Light
1471 blue trace shows the response persisted in the presence of blockers of spiking and
1472 nicotinic transmission (1 μ M tetrodotoxin (TTX), 250 μ M mecamylamine (MEC)).
1473 Overall response magnitude actually grew larger. (C) Whole cell recordings showing
1474 MBON responses to DAN photostimulation. Dark blue trace shows a representative
1475 single trial in control conditions, where DAN photostimulation (2 msec) elicits a strong
1476 depolarization, driving the cell across spike threshold. Light blue trace shows a single
1477 trial of the response from the same cell following addition of the blockers as in B, again
1478 indicating that the evoked response does not require spikes or nicotinic transmission. As
1479 with imaging, the depolarization was larger in the presence of the blockers. Insert in
1480 upper right shows the initial portion of the trace at an expanded time scale. (D) Average
1481 MBON responses to DAN photostimulation before and after blocker addition (mean +
1482 SEM of n = 4 whole cell recordings). The responses prior to blocker addition were low-
1483 pass filtered to eliminate spikes before averaging. (E) MBON responses to DAN
1484 photostimulation in the presence of TTX and MEC (light blue; mean + SEM from n=5
1485 recordings) were strongly diminished by the application of the dopamine receptor
1486 antagonist SCH 23390 (100 μ M; magenta). (F) MBON response amplitudes during
1487 wash-in of SCH 23390. Peak amplitudes were normalized to the mean of the first three
1488 trials in each cell. Error bars: SEM.

1489
1490 **Figure 7 – figure supplement 1:** KC>MBON transmission is blocked under the
1491 conditions used to test DAN>MBON connectivity. (A) Experimental schematic.
1492 ChrimsonR-expressing α/β KCs were photostimulated for 100 msec, and MBON- $\alpha 1$
1493 responses measured with whole-cell recordings. (B) Representative recordings from a
1494 single cell. Black trace shows response in the absence of blockers; note the much shorter
1495 response time course compared to DAN stimulation (Figure 7). Blue trace shows the
1496 response when spiking is blocked (1 μ M tetrodotoxin (TTX)), indicating a strong
1497 monosynaptic connection. This response was effectively blocked by the addition of the
1498 nicotinic antagonist 250 μ M mecamylamine (MEC), red trace. (C) Average responses
1499 (mean \pm SEM; n = 6). The small upward deflection remaining in the presence of TTX
1500 and MEC (red) was also observed in flies that did not express ChrimsonR (green trace; n
1501 = 6 with TTX and MEC), indicating that it is brought about by the light itself, not from
1502 optogenetic stimulation. Similar photoelectric effects have been observed by others
1503 (Cardin et al., 2010).

1504
1505

1506 **Figure 8:** Behavioral consequences of DAN activation.

1507 (A) Female flies expressing CsChrimson in PAM- $\alpha 1$ (MB043C x 20xUAS-IVS-
1508 CsChrimson-mVenus in attP18) were starved for 48 h and then trained to form an
1509 appetitive odor memory by exposure to an odor (odor A) while delivering thirty 1 s
1510 pulses of red light (1s ON + 1s OFF), followed by exposure to a second odor (odor B) in
1511 the dark. The conditioned odor response was tested immediately after the training with or
1512 without the activating red light (see Methods for details). Experiments were done
1513 reciprocally: In one group of flies, odor A and B were 3-octanol and 4-
1514 methylcyclohexanol, respectively, while in a second group of flies, the odors were
1515 reversed. The performance index (PI) is defined as [(number of flies in the odor A
1516 quadrants) - (number of flies in odor B quadrants)]/(total number of flies). The average PI
1517 of reciprocal experiments during the test period is plotted. The odor delivery started at 2 s
1518 and the arena was filled with odor by 5 s. Thick lines and error bars represent mean and
1519 SEM, respectively. Mean PI of the final 30 s of each test period was significantly
1520 ($p < 0.05$; N=8; Mann-Whitney U test) lower when activation light was ON (red; 1s ON +
1521 1s OFF) compared to the PI of flies tested in dark (gray). (B) The conditioned response
1522 was also reduced in single odor conditioning ($p < 0.05$; N=8; Mann-Whitney U test). Flies
1523 were trained in the similar protocol as in (A), but odors A and B were 3-octanol and air.
1524 Because memory scores tend to be lower in this type of single odor conditioning, training
1525 was repeated three times. (C) Female flies expressing CsChrimson-mVenus in PPL1- $\alpha 3$
1526 (MB630B x 20xUAS-IVS-CsChrimson-mVenus in attP18) were trained ten times with
1527 15 min inter-training intervals to form an aversive odor memory and then tested 1 d later.
1528 The conditioned response was significantly reduced by DAN activation during test
1529 ($p < 0.05$; N=12; Mann-Whitney U test). Note that the $\alpha 3$ compartment has a slow
1530 memory acquisition rate and the same 60 s pairing of odor and thirty times 1 s activation
1531 was insufficient to induce significant immediate memory (Aso and Rubin, 2016). Thus
1532 the reduced conditioned odor preference is likely due to the suppression of memory
1533 expression rather than formation of a new odor memory for the control odor. (D)
1534 Untrained female flies were tested for preference to optogenetic activation of DANs.
1535 From 30–60 s, two of the quadrants (Q2&3) were continuously illuminated with red LED

1536 lights to activate CsChrimson-containing neurons; from 90–120 s, the other two
1537 quadrants (Q1 & 4) were illuminated instead. The preference index was calculated based
1538 on the distribution of flies during the last 5 s of these two test periods (Aso et al. 2014b).
1539 Flies expressing CsChrimson in PPL1- α 3 (MB630B) or PPL- α 3 and additional PPL1
1540 DANs (MB065B and MB504B) preferred the illuminated quadrants, whereas the control
1541 genotype (empty split-GAL4 driver, pBDP-p65ADZp in attP40; pBDP-GAL4ZpDBD in
1542 attP2/20xUAS-CsChrimson-mVenus in attP18) showed a very slight preference for
1543 illuminated quadrants. * and ** denotes $p < 0.05$ or $p < 0.01$ respectively by Kruskal
1544 Wallis One way ANOVA followed by Dunn's post-test for comparison between control
1545 and experimental genotype. N = 13–20.

1546

1547

1548 **Figure 9:** Distributions of synapses between the feedforward glutamatergic MBON-
1549 β 1> α and GABAergic MBON- γ 1pedc> α / β , and the dendrites of an MBON in each
1550 compartment.

1551 (A-C) Synaptic inputs from MBON- β 1> α are shown as black dots and are distributed
1552 uniformly over the dendrites of MBON- α 3 (A) and MBON- α 2sc (B). In contrast, its
1553 synaptic inputs to MBON- α 1 are located more closely to the root of the dendrites(C).
1554 (D) Synapses of MBON- β 1> α onto MBON- γ 1pedc> α / β in the α 3 and α 2 compartments
1555 are shown; we lack data for these synapses in α 1. (E-G) The numbers of synapses are
1556 plotted (on a log scale) as a function of distance from the root of MBON's dendrites,
1557 the point where the dendrites become a single axonal fiber (indicated by arrows in
1558 A-C). Arrows indicate average of all positions.

1559

1560

1561 **Figure 10:** Summary diagram of the connectome reconstruction of the α lobe.

1562 (A) The synaptic connectivity in each compartment are shown as arrows whose
1563 width is indicative of the number of synapses connecting the corresponding cell
1564 types. The arrows are color-coded as follows: DANs, green; MBONs with dendrites in
1565 the α 1, α 2 and α 3 compartments, purple; the feedforward MBON- γ 1pedc> α / β , dark
1566 blue; the feedforward MBON- β 1> α , magenta; DPM, brown; and APL, light blue.
1567 Arrowheads indicate the main presynaptic sites of each neuron type. The names of
1568 cell types (shown in the rectangles with rounded corners) are color coded to reflect
1569 the major neurotransmitter of the cell: black, dopamine; orange, acetylcholine;
1570 green, glutamate; blue, GABA. The transmitter for MBON- α 2sp is unknown (name is
1571 shown in grey), and for DPM (name shown in brown) is 5HT, GABA and the
1572 neuropeptide amnesiac. The correspondence of number of connections and line
1573 thickness is as follows: no line is shown when there are less than 5 connections; 5
1574 connections, 2 pt line; 50 connections, 4 pt line; 15000 connections, 35 pt line; with
1575 line widths interpolated between these values using a log scale. Precise numbers
1576 can be found in the Tables 2-8 and Supplementary file 1. For some connections, such
1577 as the connections to and from KCs of APL, DPM, MBON- γ 1pedc> α / β , MBON-
1578 β 1> α and KCs, we have pooled the data from all three α -lobe compartments and
1579 present them in the lower rectangle labelled α lobe. We similarly pooled data on
1580 synapses between MBON- γ 1pedc> α / β and MBON- β 1> α and from MBON- γ 1pedc> α / β

1581 to APL that was derived from counts in the α 2 and α 3 compartments. When more
1582 than one cell of a given type is present, such as the two MBON- α 3 cells, the synapse
1583 counts for each cell have been added in determining line widths. The connection
1584 from MBON- γ 1pedc> α/β to MBON- α 1 is shown as a faint arrow because the EM
1585 reconstruction failed to identify MBON- γ 1pedc> α/β in the α 1 compartment (see text),
1586 although the presence of its arbors is indicated by light level data (Aso et al. 2014a).

1587

1588

1589 **Supplementary File 1:** This file unzips to a directory containing the connectome
1590 and synapse locations in human readable (JSON) format, and the program used to
1591 analyze this data for this paper. The synapse locations, both pre-and post-synaptic,
1592 are in file "synapse.json". The mapping of neuron identifiers to names is in file
1593 "annotations-body.json". Files annotating which synapses are in alpha lobes 1,2, or
1594 3, and in the alpha lobe as a whole, are in bool-lobe-N.json, where N is the lobe and
1595 100 is used for the alpha lobe as a whole. The program used to analyze these data is
1596 included as "s.cpp".

1597

Cell types	Clear vesicles	Dense-core vesicles (nm)	Synaptic motif
KCs	+	74.6 ± 10.1	Convergent (rosette) synapses Polyadic to modulatory cells, occasionally monad
PPL1- α 3	+	107.8 ± 19.6	Polyadic
PPL1- $\alpha'2\alpha$ 2	+	84.4 ± 14.9	Polyadic
PAM- α 1	+	80.3 ± 10.8	Polyadic
MBON- β 1> α	+	83.2 ± 16.9	Polyadic
MBON- γ 1pedc> α/β	+	-	Polyadic
APL	+	82.8 ± 12.8	Polyadic
DPM	+	80.8 ± 12.2	Polyadic
SIFamide	-	125.5 ± 26.4	Monad/Dyad

1598

1599 **Table 1:** Types of synaptic vesicles and synaptic motifs in different neuron types. The size
 1600 estimates for dense core vesicles (mean ± SD) were based on counting 100 vesicles for each cell
 1601 type. Clear vesicles size 40-50 nm in diameter and all appear to have uniform shape and size.
 1602

Postsynaptic MBON	Number of pre-synaptic KCs	Total number of KC>MBON synapses	Mean number of KC>MBON synapses per KC	Number and (percent) of KC>MBON synapses for α/β sc	Number and (percent) of KC>MBON synapses for α/β p
MBON- α 3-A	948	12770	13.47	12278 (96.1%)	492 (3.9%)
MBON- α 3-B	948	13129	13.85	12425 (94.6%)	704 (5.4%)
MBON- α 2p3p-A	236	1311	5.56	325 (24.8%)	986 (75.2%)
MBON- α 2p3p-B	168	692	4.12	113 (16.3%)	579 (83.7%)
MBON- α 2sc	909	11281	12.41	11214 (99.4%)	67 (0.6%)
MBON - α 2sp	823	3529	4.29	2835 (80.3%)	694 (19.7%)
MBON- α 1-A	949	9303	9.80	8239 (88.6%)	1064 (11.4%)
MBON- α 1-B	949	9286	9.79	8178 (88.1%)	1108 (11.9%)

1603

1604

Table 2: Direct connections from KCs to MBONs. Synapses per KC is the mean over all connected KCs.

1605

1606

1607

1608

1609

Neuron	KC α/β s	KC α/β c(o)	KC α/β c(i)	KC α/β p
MBON- α 3-A	480/480 x 15.88	131/132 x 13.27	259/259 x 11.25	78/78 x 6.31
MBON- α 3-B	480/480 x 16.32	131/132 x 12.60	259/259 x 11.36	78/78 x 9.03
MBON- α 2p3p-A	138/480 x 2.17	15/132 x 1.27	5/259 x 1.20	78/78 x 12.64
MBON- α 2p3p-B	80/480 x 1.27	9/132 x 1.11	1/259 x 1.00	78/78 x 7.42
MBON- α 2sc	480/480 x 14.13	132/132 x 13.67	259/259 x 10.14	38/78 x 1.76
MBON- α 2sp	470/480 x 4.33	130/132 x 3.58	145/259 x 2.30	78/78 x 8.90
MBON- α 1-A	480/480 x 10.73	132/132 x 7.99	259/259 x 7.85	78/78 x 13.64
MBON- α 1-B	480/480 x 10.86	132/132 x 8.57	259/259 x 7.09	78/78 x 14.21

1610

1611 **Table 3:** How output neurons sample from KCs. KC α/β s is surface, KC α/β c(i) is inner core, KC
 1612 α/β c(o) outer core and KC α/β p is posterior. Each entry is of the form A/B x C, where A is the
 1613 number of contributing KCs out of B of that type, and C is the average number of KC>MBON
 1614 synapses, for those that are connected. In general the connections are both numerous and
 1615 complete. However, some output neurons from α 2 sample only from a subset of the available
 1616 KCs, and only with weak connections.

1617

Presynaptic DAN	Number of postsynaptic KCs	Total synapse number	Mean synapses per KC	Number of synapses to α/β sc KCs	Number of synapses to α/β p KCs
PPL1- α 3-A	706	1336	1.89	1226 (91.8%)	110 (8.2%)
PPL1- α 3-B	786	1648	2.10	1515 (91.9%)	133 (8.1%)
PPL1- α 2 α 2-A	455	653	1.44	502 (76.9%)	151 (23.1%)
PPL1- α 2 α 2-B	484	813	1.68	589 (72.4%)	224 (27.6%)
PAM- α 1-A	158	182	1.15	164 (90.1%)	18 (9.9%)
PAM- α 1-B	121	134	1.11	129 (96.3%)	5 (3.7%)
PAM- α 1-C	149	181	1.21	128 (70.7%)	53 (29.3%)
PAM- α 1-D	149	170	1.14	159 (93.5%)	11 (6.5%)
PAM- α 1-E	163	177	1.09	161 (91.0%)	16 (9.0%)
PAM- α 1-F	135	151	1.12	137 (90.7%)	14 (9.3%)
PAM- α 1-G	123	138	1.11	120 (87.0%)	18 (13.0%)
PAM- α 1-H	95	105	1.10	102 (97.1%)	3 (2.9%)
PAM- α 1-I	71	81	1.14	54 (66.7%)	27 (33.3%)
PAM- α 1-J	100	112	1.12	107 (95.5%)	5 (4.5%)
PAM- α 1-K	40	43	1.07	40 (93.0%)	3 (7.0%)
PAM- α 1-L	89	95	1.07	69 (72.6%)	26 (27.4%)
PAM- α 1-M	148	179	1.21	166 (92.7%)	13 (7.3%)
PAM- α 1-N	78	125	1.60	30 (24.0%)	95 (76.0%)
PAM- α 1-O	52	56	1.08	46 (82.1%)	10 (17.9%)
PAM- α 1-P	61	82	1.34	19 (23.2%)	63 (76.8%)

1618

1619 **Table 4:** Direct connections from DANs to KCs. Thick lines divide compartments. Mean
 1620 synapses per KC is the number of DAN to KC for that presynaptic DAN cell type /number of
 1621 postsynaptic KCs. The right two columns specify the number of postsynaptic KC-sc and KC-p;
 1622 the percentages are the fraction of DAN-KC synapses for that class of KC.

1623

		Number of synapses where APL is		Number of synapses where DPM is		Number of synapses where SIFamide is		Number of synapses where MBON- $\beta 1>\alpha$ is		Number of synapses where MBON- $\gamma 1pedc>\alpha/\beta^*$ is	
		Post-Synaptic	Pre-synaptic	Post-synaptic	Pre-synaptic	Post-synaptic	Pre-synaptic	Post-synaptic	Pre-synaptic	Post-synaptic	Pre-synaptic
	KCs (α lobe)	9128	4124	7224	1978	68	15	325	320	102	0
All α lobe	APL	-	-	39	166	0	0	76	2	0	98
	DPM	166	39	-	-	0	1	73	15	4	1
	SIFamide	0	0	1	0	-	-	0	0	0	0
	MBON- $\beta 1>\alpha$	2	76	15	73	0	0	-	-	22	6
	MBON- $\gamma 1pedc>\alpha/\beta-R^*$	77	0	0	3	0	0	3	21	-	-
	MBON- $\gamma 1pedc>\alpha/\beta-L^*$	21	0	1	1	0	0	3	1	-	-
$\alpha 3$	KCs ($\alpha 3$)	3244	1443	3213	922	42	7	152	136	30	19
	PPL1- $\alpha 3$ -A	10	0	24	12	0	0	0	1	0	3
	PPL1- $\alpha 3$ -B	13	0	29	31	0	0	1	0	0	3
	MBON- $\alpha 3$ -A	0	0	0	4	0	0	0	107	0	60
	MBON- $\alpha 3$ -B	0	0	0	4	0	0	0	95	0	61
$\alpha 2$	KCs ($\alpha 2$)	3144	1276	2262	643	25	8	84	49	69	23
	PPL1- $\alpha' 2\alpha 2$ -A	38	0	58	33	0	0	0	6	0	1
	PPL1- $\alpha' 2\alpha 2$ -B	45	0	44	46	0	0	1	12	0	2
	MBON- $\alpha 2p3p$ -A	0	0	0	3	0	0	0	62	0	17
	MBON- $\alpha 2p3p$ -B	0	0	0	3	0	0	0	47	0	10
	MBON- $\alpha 2sc$	0	0	0	21	0	2	0	80	0	69
$\alpha 1$	KCs ($\alpha 1$)	2740	1404	1749	413	1	0	89	135	*	
	PAM- $\alpha 1$ (16)	21	0	22	80	0	0	85	84		
	MBON- $\alpha 1$ -A	0	29	0	134	0	0	0	132		
	MBON- $\alpha 1$ -B	0	34	0	111	0	0	0	156		

1624

1625 **Table 5:** Connections of cells that innervate the α lobe. The top section shows connectivity to
1626 cells that innervate all three compartments. Lower sections are the compartment specific
1627 connectivity. Bold lines separate compartments, with $\alpha 3$ on top. *We were unable to identify
1628 with certainty the arbor of MBON- $\gamma 1pedc>\alpha/\beta$ in $\alpha 1$ and so no counts of synapses for this neuron
1629 in $\alpha 1$ are included (see text).

1630

1631

Presynaptic DANs	Postsynaptic MBONs	Total synaptic counts	Percent
PPL1- α 3 (2)	MBON- α 3-A	456	3.57%
	MBON- α 3-B	451	3.43%
PPL1- α' 2 α 2 (2)	MBON- α 2p3p-A	26	1.95%
	MBON- α 2p3p-B	12	1.66%
	MBON- α 2sc	246	2.18%
	MBON - α 2sp	91	2.57%
PAM- α 1 (16)	MBON- α 1-A	727	7.77%
	MBON- α 1-B	736	7.90%

1632

1633

Table 6: Direct connections from DANs to MBONs in the same compartment. Dark lines separate the compartments, with α 3 on top. All MBONs in the α lobe share this circuit motif, though with varying strengths. For each MBON, the absolute number of DAN to MBON synapses is shown as well as the percentage that number represents of synapses from KCs received by that MBON.

1634

1635

1636

1637

1638

Postsynaptic DAN	Number of presynaptic KCs	Total synapse number	Mean synapses per KC	Number of synapses from KC α/β sc	Number of synapses from KC α/β p
PPL1- α 3-A	883	2822	3.20	2706 (95.9%)	116 (4.1%)
PPL1- α 3-B	834	2215	2.66	2155 (97.3%)	60 (2.7%)
PPL1- α '2 α 2-A	488	809	1.66	728 (90.0%)	81 (10.0%)
PPL1- α '2 α 2-B	480	791	1.65	683 (86.3%)	108 (13.7%)
PAM- α 1-A	209	251	1.20	239 (95.2%)	12 (4.8%)
PAM- α 1-B	239	332	1.39	320 (96.4%)	12 (3.6%)
PAM- α 1-C	218	283	1.30	212 (74.9%)	71 (25.1%)
PAM- α 1-D	191	256	1.34	239 (93.4%)	17 (6.6%)
PAM- α 1-E	194	254	1.31	248 (97.6%)	6 (2.4%)
PAM- α 1-F	193	241	1.25	235 (97.5%)	6 (2.5%)
PAM- α 1-G	143	171	1.20	156 (91.2%)	15 (8.8%)
PAM- α 1-H	156	176	1.13	170 (96.6%)	6 (3.4%)
PAM- α 1-I	156	212	1.36	155 (73.1%)	57 (26.9%)
PAM- α 1-J	124	149	1.20	148 (99.3%)	1 (0.7%)
PAM- α 1-K	86	97	1.13	87 (89.7%)	10 (10.3%)
PAM- α 1-L	174	215	1.24	161 (74.9%)	54 (25.1%)
PAM- α 1-M	218	266	1.22	252 (94.7%)	14 (5.3%)
PAM- α 1-N	49	59	1.20	26 (44.1%)	33 (55.9%)
PAM- α 1-O	50	56	1.12	47 (83.9%)	9 (16.1%)
PAM- α 1-P	29	36	1.24	12 (33.3%)	24 (66.7%)

1639

1640

Table 7: Connections from KCs to DANs. Thick lines divide compartments, with α 3 at the top. There are two DANs each in the α 3 and α 2 compartments, and 16 in α 1. Mean synapses per KC is the number of KC>DAN synapses/number of KCs making synapses to DANs. The left two columns specify the number of presynaptic KC α/β sc and KC α/β p, respectively; the percentages are the fraction of KC>DAN synapses provided by that class of KC.

1641

1642

1643

1644

1645

1646

Compartment	From	To			
		KC $\alpha/\beta p$	KC $\alpha/\beta s$	KC $\alpha/\beta c(o)$	KC $\alpha/\beta c(i)$
α_3	KC $\alpha/\beta p$	18.0 x 1.29	3.4 x 1.10		
α_2		13.5 x 1.31	1.6 x 1.12		
α_1		23.5 x 1.30	4.0 x 1.09		
α_3	KC $\alpha/\beta s$		34.0 x 1.22 16.6 x 1.18 22.8 x 1.22	2.7 x 1.11 1.3 x 1.13 2.0 x 1.13	
α_2					
α_1					
α_3	KC $\alpha/\beta c(o)$		9.0 x 1.13 4.4 x 1.12 7.1 x 1.12	12.5 x 1.21 9.5 x 1.18 12.0 x 1.14	7.3 x 1.16 3.6 x 1.12 5.4 x 1.10
α_2					
α_1					
α_3	KC $\alpha/\beta c(i)$			4.1 x 1.16 1.8 x 1.12 2.7 x 1.11	21.5 x 1.22 13.7 x 1.17 22.2 x 1.23
α_2					
α_1					

1647

1648

1649

1650

1651

1652

1653

1654

1655

1656

1657

1658

Table 8: KC to KC connections in the α lobe. Each box has 3 entries, one each for the three compartments. Each entry is of the form A x B, where A is the average number of connected presynaptic cells (averaged over all KCs) and B is the average number of synapses between cells that are connected. No pairs are strongly connected, but there are many connections. Squares with less than 1 synapse per KC on average are left blank.

1659
1660
1661 **Acknowledgements.**
1662 We thank Emily Nielson for assistance with the figures, Matt Staley and John
1663 Rappole for help in adding narration to the videos, and Davi Bock, Albert Cardona,
1664 Joshua Dudman, Bertrum Gerber, Daisuke Hattori, Gregory Jefferis, Hiromu
1665 Tanimoto, Scott Waddell and Marta Zlatic for comments on the manuscript.
1666
1667

1668 **References**

1669

- 1670 AKALAL, D. B., YU, D. & DAVIS, R. L. 2011. The long-term memory trace formed in
1671 the *Drosophila* alpha/beta mushroom body neurons is abolished in long-
1672 term memory mutants. *J Neurosci*, 31, 5643-7.
- 1673 AOSAKI, T., KIUCHI, K. & KAWAGUCHI, Y. 1998. Dopamine D1-like receptor
1674 activation excites rat striatal large spiny neurons in vitro. *J Neurosci*, 18,
1675 5180-90.
- 1676 ARDIEL, E. L. & RANKIN, C. H. 2010. An elegant mind: learning and memory in
1677 *Caenorhabditis elegans*. *Learn Mem*, 17, 191-201.
- 1678 ASO, Y., GRUBEL, K., BUSCH, S., FRIEDRICH, A. B., SIWANOWICZ, I. & TANIMOTO, H.
1679 2009. The mushroom body of adult *Drosophila* characterized by GAL4
1680 drivers. *J Neurogenet*, 23, 156-72.
- 1681 ASO, Y., HATTORI, D., YU, Y., JOHNSTON, R. M., IYER, N. A., NGO, T. T., DIONNE, H.,
1682 ABBOTT, L. F., AXEL, R., TANIMOTO, H. & RUBIN, G. M. 2014a. The neuronal
1683 architecture of the mushroom body provides a logic for associative learning.
1684 *Elife*, 3, e04577.
- 1685 ASO, Y., HERB, A., OGUETA, M., SIWANOWICZ, I., TEMPLIER, T., FRIEDRICH, A. B.,
1686 ITO, K., SCHOLZ, H. & TANIMOTO, H. 2012. Three dopamine pathways induce
1687 aversive odor memories with different stability. *PLoS Genet*, 8, e1002768.
- 1688 ASO, Y. & RUBIN, G. M. 2016. Dopaminergic neurons write and update memories
1689 with cell-type-specific rules. *Elife*, 5.
- 1690 ASO, Y., SITARAMAN, D., ICHINOSE, T., KAUN, K. R., VOGT, K., BELLIArt-GUERIN, G.,
1691 PLACAIS, P. Y., ROBIE, A. A., YAMAGATA, N., SCHNAITMANN, C., ROWELL, W.
1692 J., JOHNSTON, R. M., NGO, T. T., CHEN, N., KORFF, W., NITABACH, M. N.,
1693 HEBERLEIN, U., PREAT, T., BRANSON, K. M., TANIMOTO, H. & RUBIN, G. M.
1694 2014b. Mushroom body output neurons encode valence and guide memory-
1695 based action selection in *Drosophila*. *Elife*, 3, e04580.
- 1696 ASO, Y., SIWANOWICZ, I., BRACKER, L., ITO, K., KITAMOTO, T. & TANIMOTO, H.
1697 2010. Specific dopaminergic neurons for the formation of labile aversive
1698 memory. *Curr Biol*, 20, 1445-51.
- 1699 BARNSTEDT, O., OWALD, D., FELSENBURG, J., BRAIN, R., MOSZYNSKI, J. P., TALBOT,
1700 C. B., PERRAT, P. N. & WADDELL, S. 2016. Memory-Relevant Mushroom Body
1701 Output Synapses Are Cholinergic. *Neuron*, 89, 1237-47.
- 1702 BERRY, J. A., CERVANTES-SANDOVAL, I., CHAKRABORTY, M. & DAVIS, R. L. 2015.
1703 Sleep Facilitates Memory by Blocking Dopamine Neuron-Mediated
1704 Forgetting. *Cell*, 161, 1656-67.
- 1705 BERRY, J. A., CERVANTES-SANDOVAL, I., NICHOLAS, E. P. & DAVIS, R. L. 2012.
1706 Dopamine is required for learning and forgetting in *Drosophila*. *Neuron*, 74,
1707 530-42.
- 1708 BLUM, A. L., LI, W., CRESSY, M. & DUBNAU, J. 2009. Short- and long-term memory in
1709 *Drosophila* require cAMP signaling in distinct neuron types. *Curr Biol*, 19,
1710 1341-50.

- 1711 BOTO, T., LOUIS, T., JINDACHOMTHONG, K., JALINK, K. & TOMCHIK, S. M. 2014.
1712 Dopaminergic modulation of cAMP drives nonlinear plasticity across the
1713 Drosophila mushroom body lobes. *Curr Biol*, 24, 822-31.
- 1714 BOUZAIANE, E., TRANNOY, S., SCHEUNEMANN, L., PLACAIS, P. Y. & PREAT, T. 2015.
1715 Two independent mushroom body output circuits retrieve the six discrete
1716 components of Drosophila aversive memory. *Cell Rep*, 11, 1280-92.
- 1717 BURKE, C. J., HUETTEROTH, W., OWALD, D., PERISSE, E., KRASHES, M. J., DAS, G.,
1718 GOHL, D., SILIES, M., CERTEL, S. & WADDELL, S. 2012. Layered reward
1719 signalling through octopamine and dopamine in Drosophila. *Nature*, 492,
1720 433-7.
- 1721 BUSH, R. R. & MOSTELLER, F. 1951. A mathematical model for simple learning.
1722 *Psychol Rev*, 58, 313-23.
- 1723 CAMPBELL, R. A. A., HONEGGER, K. S., QIN, H. T., LI, W. H., DEMIR, E. & TURNER, G. C.
1724 2013. Imaging a Population Code for Odor Identity in the Drosophila
1725 Mushroom Body. *Journal of Neuroscience*, 33, 10568-10581.
- 1726 CARDIN, J. A., CARLEN, M., MELETIS, K., KNOBLICH, U., ZHANG, F., DEISSEROOTH, K.,
1727 TSAI, L. H. & MOORE, C. I. 2010. Targeted optogenetic stimulation and
1728 recording of neurons *in vivo* using cell-type-specific expression of
1729 Channelrhodopsin-2. *Nat Protoc*, 5, 247-54.
- 1730 CARON, S. J., RUTA, V., ABBOTT, L. F. & AXEL, R. 2013. Random convergence of
1731 olfactory inputs in the Drosophila mushroom body. *Nature*, 497, 113-7.
- 1732 CASSENAER, S. & LAURENT, G. 2012. Conditional modulation of spike-timing-
1733 dependent plasticity for olfactory learning (vol 482, pg 47, 2012). *Nature*,
1734 487.
- 1735 CERVANTES-SANDOVAL, I. & DAVIS, R. L. 2012. Distinct traces for appetitive versus
1736 aversive olfactory memories in DPM neurons of Drosophila. *Curr Biol*, 22,
1737 1247-52.
- 1738 CERVANTES-SANDOVAL, I., PHAN, A., CHAKRABORTY, M. & DAVIS, R. L. 2017.
1739 Reciprocal synapses between mushroom body and dopamine neurons form a
1740 positive feedback loop required for learning. *Elife*, 6.
- 1741 CLARIDGE-CHANG, A., ROORDA, R. D., VRONTOU, E., SJULSON, L., LI, H., HIRSH, J. &
1742 MIESENBOCK, G. 2009. Writing memories with light-addressable
1743 reinforcement circuitry. *Cell*, 139, 405-15.
- 1744 COHN, R., MORANTTE, I. & RUTA, V. 2015. Coordinated and Compartmentalized
1745 Neuromodulation Shapes Sensory Processing in Drosophila. *Cell*, 163, 1742-
1746 55.
- 1747 CRITTENDEN, J. R., SKOULAKIS, E. M., HAN, K. A., KALDERON, D. & DAVIS, R. L. 1998.
1748 Tripartite mushroom body architecture revealed by antigenic markers. *Learn
1749 Mem*, 5, 38-51.
- 1750 CROCKER, A., GUAN, X. J., MURPHY, C. T. & MURTHY, M. 2016. Cell-Type-Specific
1751 Transcriptome Analysis in the Drosophila Mushroom Body Reveals Memory-
1752 Related Changes in Gene Expression. *Cell Rep*, 15, 1580-96.
- 1753 DAS, G., KLAPPENBACH, M., VRONTOU, E., PERISSE, E., CLARK, C. M., BURKE, C. J. &
1754 WADDELL, S. 2014. Drosophila learn opposing components of a compound
1755 food stimulus. *Curr Biol*, 24, 1723-30.

- 1756 DE BELLE, J. S. & HEISENBERG, M. 1994. Associative odor learning in *Drosophila*
1757 abolished by chemical ablation of mushroom bodies. *Science*, 263, 692-5.
- 1758 DEAN, P., PORRILL, J., EKEROT, C. F. & JORNTELL, H. 2010. The cerebellar
1759 microcircuit as an adaptive filter: experimental and computational evidence.
1760 *Nat Rev Neurosci*, 11, 30-43.
- 1761 DUBNAU, J., GRADY, L., KITAMOTO, T. & TULLY, T. 2001. Disruption of
1762 neurotransmission in *Drosophila* mushroom body blocks retrieval but not
1763 acquisition of memory. *Nature*, 411, 476-80.
- 1764 EICHLER, K., LI, F., LITWIN-KUMAR, A., PARK, Y., ANDRADE, I., SCHNEIDER-MIZELL,
1765 C., SAUMWEBER, T., HUSER, A., ESCHBACH, C., GERBER, B., FETTER, R. D.,
1766 TRUMAN, J. W., PRIEBE, C., ABBOTT, L. F., THUM, A., ZLATIC, M. & CARDONA,
1767 A. 2017 (in press). The complete wiring diagram of the larval *Drosophila*
1768 mushroom body. *Nature*.
- 1769 ERBER, J., MASUHR, T. & MENZEL, R. 1980. Localization of short-term memory in
1770 the brain of the bee, *Apis mellifera*. *Physiological Entomology*, 5.
- 1771 FRANK, D. D., JOUANDET, G. C., KEARNEY, P. J., MACPHERSON, L. J. & GALLIO, M.
1772 2015. Temperature representation in the *Drosophila* brain. *Nature*, 519, 358-
1773 61.
- 1774 GARRIS, P. A., CIOLKOWSKI, E. L., PASTORE, P. & WIGHTMAN, R. M. 1994. Efflux of
1775 dopamine from the synaptic cleft in the nucleus accumbens of the rat brain. *J
1776 Neurosci*, 14, 6084-93.
- 1777 GERVASI, N., TCHENIO, P. & PREAT, T. 2010. PKA dynamics in a *Drosophila* learning
1778 center: coincidence detection by rutabaga adenylyl cyclase and spatial
1779 regulation by dunce phosphodiesterase. *Neuron*, 65, 516-29.
- 1780 GONON, F. 1997. Prolonged and extrasynaptic excitatory action of dopamine
1781 mediated by D1 receptors in the rat striatum *in vivo*. *J Neurosci*, 17, 5972-8.
- 1782 GRUNTMAN, E. & TURNER, G. C. 2013. Integration of the olfactory code across
1783 dendritic claws of single mushroom body neurons. *Nat Neurosci*, 16, 1821-9.
- 1784 HAN, K. A., MILLAR, N. S., GROTEWIEL, M. S. & DAVIS, R. L. 1996. DAMB, a novel
1785 dopamine receptor expressed specifically in *Drosophila* mushroom bodies.
1786 *Neuron*, 16, 1127-35.
- 1787 HAYNES, P. R., CHRISTMANN, B. L. & GRIFFITH, L. C. 2015. A single pair of neurons
1788 links sleep to memory consolidation in *Drosophila melanogaster*. *Elife*, 4.
- 1789 HEISENBERG, M. 2003. Mushroom body memoir: From maps to models. *Nature
1790 Reviews Neuroscience*, 4, 266-275.
- 1791 HEISENBERG, M., BORST, A., WAGNER, S. & BYERS, D. 1985. *Drosophila* mushroom
1792 body mutants are deficient in olfactory learning. *J Neurogenet*, 2, 1-30.
- 1793 HIGE, T., ASO, Y., MODI, M. N., RUBIN, G. M. & TURNER, G. C. 2015a. Heterosynaptic
1794 Plasticity Underlies Aversive Olfactory Learning in *Drosophila*. *Neuron*, 88,
1795 985-98.
- 1796 HIGE, T., ASO, Y., RUBIN, G. M. & TURNER, G. C. 2015b. Plasticity-driven
1797 individualization of olfactory coding in mushroom body output neurons.
1798 *Nature*, 526, 258-62.
- 1799 HONEGGER, K. S., CAMPBELL, R. A. & TURNER, G. C. 2011. Cellular-resolution
1800 population imaging reveals robust sparse coding in the *Drosophila*
1801 mushroom body. *J Neurosci*, 31, 11772-85.

- 1802 HUANG, G. B. J., V. 2013. Deep and wide multiscale recursive networks for robust
1803 image labeling. *arXiv*, 1310.0354.
- 1804 HUANG, G. B. P., S. M. 2014. Identifying synapses using deep and wide multiscale
1805 recursive networks. . *arXiv*, 1409.1789.
- 1806 HUETTEROTH, W., PERISSE, E., LIN, S., KLAPPENBACH, M., BURKE, C. & WADDELL,
1807 S. 2015. Sweet taste and nutrient value subdivide rewarding dopaminergic
1808 neurons in *Drosophila*. *Curr Biol*, 25, 751-8.
- 1809 ICHINOSE, T., ASO, Y., YAMAGATA, N., ABE, A., RUBIN, G. M. & TANIMOTO, H. 2015.
1810 Reward signal in a recurrent circuit drives appetitive long-term memory
1811 formation. *Elife*, 4.
- 1812 ITO, K., AWANO, W., SUZUKI, K., HIROMI, Y. & YAMAMOTO, D. 1997. The *Drosophila*
1813 mushroom body is a quadruple structure of clonal units each of which
1814 contains a virtually identical set of neurones and glial cells. *Development*,
1815 124, 761-71.
- 1816 ITO, K., SUZUKI, K., ESTES, P., RAMASWAMI, M., YAMAMOTO, D. & STRAUSFELD, N. J.
1817 1998. The organization of extrinsic neurons and their implications in the
1818 functional roles of the mushroom bodies in *Drosophila melanogaster* Meigen.
1819 *Learn Mem*, 5, 52-77.
- 1820 KANDEL, E. R. & SCHWARTZ, J. H. 1982. Molecular biology of learning: modulation of
1821 transmitter release. *Science*, 218, 433-43.
- 1822 KATZ, W. T. & PLAZA, S. 2017. DVID. Github.
1823 6e21c1c7adb128352a2047e280189941ad682356.
1824 <https://github.com/janelia-flyem/dvid>
- 1825 KAUN, K. R., AZANCHI, R., MAUNG, Z., HIRSH, J. & HEBERLEIN, U. 2011. A *Drosophila*
1826 model for alcohol reward. *Nat Neurosci*, 14, 612-9.
- 1827 KEENE, A. C., KRASHES, M. J., LEUNG, B., BERNARD, J. A. & WADDELL, S. 2006.
1828 *Drosophila* dorsal paired medial neurons provide a general mechanism for
1829 memory consolidation. *Current Biology*, 16, 1524-1530.
- 1830 KEENE, A. C., STRATMANN, M., KELLER, A., PERRAT, P. N., VOSSHALL, L. B. &
1831 WADDELL, S. 2004. Diverse odor-conditioned memories require uniquely
1832 timed dorsal paired medial neuron output. *Neuron*, 44, 521-33.
- 1833 KIM, H. F., GHAZIZADEH, A. & HIKOSAKA, O. 2015. Dopamine Neurons Encoding
1834 Long-Term Memory of Object Value for Habitual Behavior. *Cell*, 163, 1165-75.
- 1835 KIM, Y. C., LEE, H. G. & HAN, K. A. 2007. D1 dopamine receptor dDA1 is required in
1836 the mushroom body neurons for aversive and appetitive learning in
1837 *Drosophila*. *J Neurosci*, 27, 7640-7.
- 1838 KIM, Y. C., LEE, H. G., SEONG, C. S. & HAN, K. A. 2003. Expression of a D1 dopamine
1839 receptor dDA1/DmDOP1 in the central nervous system of *Drosophila*
1840 melanogaster. *Gene Expr Patterns*, 3, 237-45.
- 1841 KIRKHART, C. & SCOTT, K. 2015. Gustatory learning and processing in the
1842 *Drosophila* mushroom bodies. *J Neurosci*, 35, 5950-8.
- 1843 KLAPOETKE, N. C., MURATA, Y., KIM, S. S., PULVER, S. R., BIRDSEY-BENSON, A., CHO,
1844 Y. K., MORIMOTO, T. K., CHUONG, A. S., CARPENTER, E. J., TIAN, Z., WANG, J.,
1845 XIE, Y., YAN, Z., ZHANG, Y., CHOW, B. Y., SUREK, B., MELKONIAN, M.,
1846 JAYARAMAN, V., CONSTANTINE-PATON, M., WONG, G. K. & BOYDEN, E. S.

- 1847 2014. Independent optical excitation of distinct neural populations. *Nature Methods*, 11, 338-46.
- 1848
1849 KRASHES, M. J., DASGUPTA, S., VREEDE, A., WHITE, B., ARMSTRONG, J. D. & WADDELL, S. 2009. A Neural Circuit Mechanism Integrating Motivational State with Memory Expression in *Drosophila*. *Cell*, 139, 416-427.
- 1850
1851 KRASHES, M. J. & WADDELL, S. 2008. Rapid consolidation to a radish and protein synthesis-dependent long-term memory after single-session appetitive olfactory conditioning in *Drosophila*. *Journal of Neuroscience*, 28, 3103-3113.
- 1852
1853 KREMER, M. C., JUNG, C., BATELLI, S., RUBIN, G. M. & GAUL, U. 2017. The glia of the adult *Drosophila* nervous system. *Glia*, 65, 606-638.
- 1854
1855 LEE, P. T., LIN, H. W., CHANG, Y. H., FU, T. F., DUBNAU, J., HIRSH, J., LEE, T. & CHIANG, A. S. 2011. Serotonin-mushroom body circuit modulating the formation of anesthesia-resistant memory in *Drosophila*. *Proc Natl Acad Sci U S A*, 108, 13794-9.
- 1856
1857 LEITCH, B. & LAURENT, G. 1996. GABAergic synapses in the antennal lobe and mushroom body of the locust olfactory system. *J Comp Neurol*, 372, 487-514.
- 1858
1859 LEVIN, L. R., HAN, P. L., HWANG, P. M., FEINSTEIN, P. G., DAVIS, R. L. & REED, R. R. 1992. The *Drosophila* learning and memory gene *rutabaga* encodes a Ca²⁺/Calmodulin-responsive adenylyl cyclase. *Cell*, 68, 479-89.
- 1860
1861 LEWIS, L. P., SIJU, K. P., ASO, Y., FRIEDRICH, A. B., BULTEEL, A. J., RUBIN, G. M. & GRUNWALD KADOW, I. C. 2015. A Higher Brain Circuit for Immediate Integration of Conflicting Sensory Information in *Drosophila*. *Curr Biol*, 25, 2203-14.
- 1862
1863 LIN, A. C., BYGRAVE, A. M., DE CALIGNON, A., LEE, T. & MIESENBOCK, G. 2014a. Sparse, decorrelated odor coding in the mushroom body enhances learned odor discrimination. *Nat Neurosci*, 17, 559-68.
- 1864
1865 LIN, H. H., LAI, J. S., CHIN, A. L., CHEN, Y. C. & CHIANG, A. S. 2007. A map of olfactory representation in the *Drosophila* mushroom body. *Cell*, 128, 1205-17.
- 1866
1867 LIN, S., OWALD, D., CHANDRA, V., TALBOT, C., HUETTEROTH, W. & WADDELL, S. 2014b. Neural correlates of water reward in thirsty *Drosophila*. *Nat Neurosci*, 17, 1536-42.
- 1868
1869 LIU, C., PLACAIS, P. Y., YAMAGATA, N., PFEIFFER, B. D., ASO, Y., FRIEDRICH, A. B., SIWANOWICZ, I., RUBIN, G. M., PREAT, T. & TANIMOTO, H. 2012. A subset of dopamine neurons signals reward for odour memory in *Drosophila*. *Nature*, 488, 512-6.
- 1870
1871 LIU, Q., YANG, X., TIAN, J., GAO, Z., WANG, M., LI, Y. & GUO, A. 2016. Gap junction networks in mushroom bodies participate in visual learning and memory in *Drosophila*. *Elife*, 5.
- 1872
1873 LIU, W. W., MAZOR, O. & WILSON, R. I. 2015. Thermosensory processing in the *Drosophila* brain. *Nature*, 519, 353-7.
- 1874
1875 LIU, X. & DAVIS, R. L. 2009. The GABAergic anterior paired lateral neuron suppresses and is suppressed by olfactory learning. *Nat Neurosci*, 12, 53-59.
- 1876
1877 LIVINGSTONE, M. S., SZIBER, P. P. & QUINN, W. G. 1984. Loss of calcium/calmodulin responsiveness in adenylyl cyclase of *rutabaga*, a *Drosophila* learning mutant. *Cell*, 37, 205-15.

- 1892 MANCINI, G. & FRONTALI, N. 1967. Fine structure of the mushroom body neuropile
 1893 of the brain of the roach, *Periplaneta americana*. *Z Zellforsch Mikrosk Anat*,
 1894 83, 334-43.
- 1895 MANCINI, G. & FRONTALI, N. 1970. On the ultrastructural localization of
 1896 catecholamines in the beta lobes (corpora pedunculata) of *Periplaneta*
 1897 *americana*. *Z Zellforsch Mikrosk Anat*, 103, 341-50.
- 1898 MAO, Z. & DAVIS, R. L. 2009. Eight different types of dopaminergic neurons
 1899 innervate the *Drosophila* mushroom body neuropil: anatomical and
 1900 physiological heterogeneity. *Front Neural Circuits*, 3, 5.
- 1901 MARDER, E., GUTIERREZ, G. J. & NUSBAUM, M. P. 2016. Complicating connectomes:
 1902 Electrical coupling creates parallel pathways and degenerate circuit
 1903 mechanisms. *Dev Neurobiol*.
- 1904 MATSUMOTO, M., SASAKI, K., SATO, M., SHOZUSHIMA, M. & TAKASHIMA, K. 1988.
 1905 Dopamine-induced depolarizing responses associated with negative slope
 1906 conductance in LB-cluster neurones of *Aplysia*. *J Physiol*, 407, 199-213.
- 1907 MCGUIRE, S. E., DESHAZER, M. & DAVIS, R. L. 2005. Thirty years of olfactory learning
 1908 and memory research in *Drosophila melanogaster*. *Prog Neurobiol*, 76, 328-
 1909 347.
- 1910 MCGUIRE, S. E., LE, P. T. & DAVIS, R. L. 2001. The role of *Drosophila* mushroom body
 1911 signaling in olfactory memory. *Science*, 293, 1330-3.
- 1912 MCGUIRE, S. E., LE, P. T., OSBORN, A. J., MATSUMOTO, K. & DAVIS, R. L. 2003.
 1913 Spatiotemporal rescue of memory dysfunction in *Drosophila*. *Science*, 302,
 1914 1765-8.
- 1915 MEDINA, J. F., REPA, J. C., MAUK, M. D. & LEDOUX, J. E. 2002. Parallels between
 1916 cerebellum and amygdala-dependent conditioning. *Nature Reviews
 1917 Neuroscience*, 3, 122-131.
- 1918 MIZUNAMI, M., WEIBRECHT, J. M. & STRAUSFELD, N. J. 1998. Mushroom bodies of
 1919 the cockroach: their participation in place memory. *J Comp Neurol*, 402, 520-
 1920 37.
- 1921 MURTHY, M., FIETE, I. & LAURENT, G. 2008. Testing odor response stereotypy in the
 1922 *Drosophila* mushroom body. *Neuron*, 59, 1009-23.
- 1923 MUSSO, P. Y., TCHEMIO, P. & PREAT, T. 2015. Delayed dopamine signaling of energy
 1924 level builds appetitive long-term memory in *Drosophila*. *Cell Rep*, 10, 1023-
 1925 31.
- 1926 OWALD, D., FELSENBERG, J., TALBOT, C. B., DAS, G., PERISSE, E., HUETTEROTH, W. &
 1927 WADDELL, S. 2015. Activity of defined mushroom body output neurons
 1928 underlies learned olfactory behavior in *Drosophila*. *Neuron*, 86, 417-27.
- 1929 PAI, T. P., CHEN, C. C., LIN, H. H., CHIN, A. L., LAI, J. S., LEE, P. T., TULLY, T. & CHIANG,
 1930 A. S. 2013. *Drosophila* ORB protein in two mushroom body output neurons is
 1931 necessary for long-term memory formation. *Proc Natl Acad Sci U S A*, 110,
 1932 7898-903.
- 1933 PAPADOPOULOU, M., CASSENAER, S., NOWOTNY, T. & LAURENT, G. 2011.
 1934 Normalization for sparse encoding of odors by a wide-field interneuron.
 1935 *Science*, 332, 721-5.

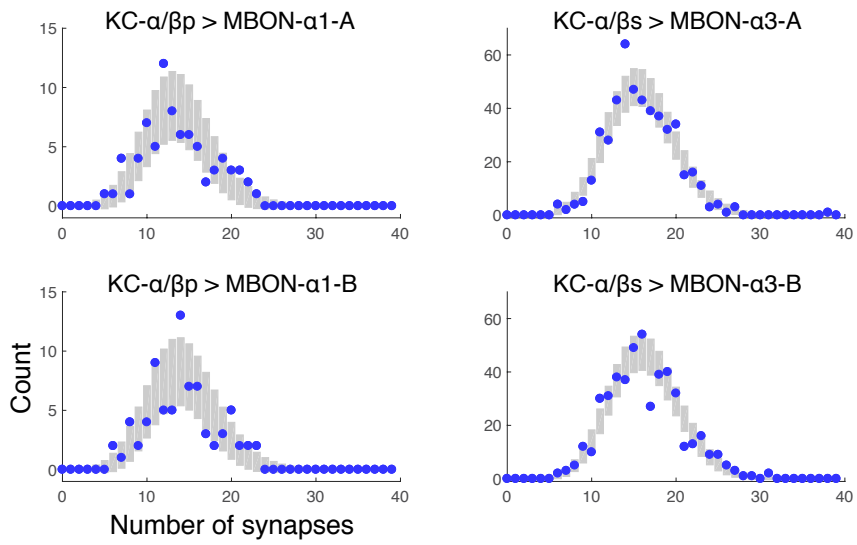
- 1936 PARAG, T., CHAKRABORTY, A., PLAZA, S. & SCHEFFER, L. 2015. A context-aware
 1937 delayed agglomeration framework for electron microscopy segmentation.
 1938 *PLoS One*, 10, e0125825.
- 1939 PARAG, T., PLAZA, S. & SCHEFFER, L. 2014. Small sample learning of superpixel
 1940 classifiers for EM segmentation. *Med Image Comput Comput Assist Interv*, 17,
 1941 389-97.
- 1942 PARK, S., SONN, J. Y., OH, Y., LIM, C. & CHOE, J. 2014. SIFamide and SIFamide
 1943 Receptor Defines a Novel Neuropeptide Signaling to Promote Sleep in
 1944 *Drosophila. Mol Cells*.
- 1945 PASCUAL, A. & PREAT, T. 2001. Localization of long-term memory within the
 1946 *Drosophila mushroom body. Science*, 294, 1115-7.
- 1947 PECH, U., POORYASIN, A., BIRMAN, S. & FIALA, A. 2013. Localization of the contacts
 1948 between Kenyon cells and aminergic neurons in the *Drosophila melanogaster*
 1949 brain using SplitGFP reconstitution. *J Comp Neurol*, 521, 3992-4026.
- 1950 PEREZ-ORIVE, J., MAZOR, O., TURNER, G. C., CASSENAER, S., WILSON, R. I. &
 1951 LAURENT, G. 2002. Oscillations and sparsening of odor representations in
 1952 the mushroom body. *Science*, 297, 359-65.
- 1953 PERISSE, E., OWALD, D., BARNSTEDT, O., TALBOT, C. B., HUETTEROTH, W. &
 1954 WADDELL, S. 2016. Aversive Learning and Appetitive Motivation Toggle
 1955 Feed-Forward Inhibition in the *Drosophila* Mushroom Body. *Neuron*, 90,
 1956 1086-99.
- 1957 PERISSE, E., YIN, Y., LIN, A. C., LIN, S., HUETTEROTH, W. & WADDELL, S. 2013.
 1958 Different kenyon cell populations drive learned approach and avoidance in
 1959 *Drosophila. Neuron*, 79, 945-56.
- 1960 PITMAN, J. L., HUETTEROTH, W., BURKE, C. J., KRASHES, M. J., LAI, S. L., LEE, T. &
 1961 WADDELL, S. 2011. A Pair of Inhibitory Neurons Are Required to Sustain
 1962 Labile Memory in the *Drosophila* Mushroom Body. *Current Biology*, 21, 855-
 1963 861.
- 1964 PLAZA, S. M. 2016a. Focused proofreading to reconstruct neural connectomes from
 1965 EM images at scale. *International Workshop on Large-Scale Annotation of*
 1966 *Biomedical Data and Expert Label Synthesis*, 249-58.
- 1967 PLAZA, S. M., SCHEFFER, L. K. & CHKLOVSKII, D. B. 2014. Toward large-scale
 1968 connectome reconstructions. *Current Opinion in Neurobiology*, 25, 201-210.
- 1969 PLAZA, S. M. B., S. E. 2016b. Large-scale electron microscopy image segmentation in
 1970 Spark. *arXiv*, 1604.00385.
- 1971 QIN, H., CRESSY, M., LI, W., CORAVOS, J. S., IZZI, S. A. & DUBNAU, J. 2012a. Gamma
 1972 neurons mediate dopaminergic input during aversive olfactory memory
 1973 formation in *Drosophila. Curr Biol*, 22, 608-14.
- 1974 QIN, H. T., CRESSY, M., LI, W. H., CORAVOS, J. S., IZZI, S. A. & DUBNAU, J. 2012b.
 1975 Gamma Neurons Mediate Dopaminergic Input during Aversive Olfactory
 1976 Memory Formation in *Drosophila. Current Biology*, 22, 608-614.
- 1977 RESCORLA, R. A. & WAGNER, A. R. 1972. A theory of Pavlovian conditioning:
 1978 Variations in the effectiveness of reinforcement and nonreinforcement.
 1979 *Classical Conditioning II*, A.H. Black & W.F. Prokasy, Eds., Appleton-Century-
 1980 Crofts., pp. 64-99..

- 1981 RIEMENSPERGER, T., VOLLMER, T., STOCK, P., BUCHNER, E. & FIALA, A. 2005.
- 1982 Punishment prediction by dopaminergic neurons in Drosophila. *Curr Biol*, 15,
- 1983 1953-60.
- 1984 ROHWEDDER, A., WENZ, N. L., STEHLE, B., HUSER, A., YAMAGATA, N., ZLATIC, M.,
- 1985 TRUMAN, J. W., TANIMOTO, H., SAUMWEBER, T., GERBER, B. & THUM, A. S.
- 1986 2016. Four Individually Identified Paired Dopamine Neurons Signal Reward
- 1987 in Larval Drosophila. *Curr Biol*, 26, 661-9.
- 1988 SCHLEYER, M., MIURA, D., TANIMURA, T. & GERBER, B. 2015. Learning the specific
- 1989 quality of taste reinforcement in larval Drosophila. *Elife*, 4.
- 1990 SCHLEYER, M., SAUMWEBER, T., NAHRENDORF, W., FISCHER, B., VON ALPEN, D.,
- 1991 PAULS, D., THUM, A. & GERBER, B. 2011. A behavior-based circuit model of
- 1992 how outcome expectations organize learned behavior in larval Drosophila.
- 1993 *Learn Mem*, 18, 639-53.
- 1994 SCHMITZ, D., SCHUCHMANN, S., FISAHN, A., DRAGUHN, A., BUHL, E. H., PETRASCH-
- 1995 PARWEZ, E., DERMIETZEL, R., HEINEMANN, U. & TRAUB, R. D. 2001. Axo-
- 1996 axonal coupling. a novel mechanism for ultrafast neuronal communication.
- 1997 *Neuron*, 31, 831-40.
- 1998 SCHROLL, C., RIEMENSPERGER, T., BUCHER, D., EHMER, J., VOLLMER, T., ERBGUTH,
- 1999 K., GERBER, B., HENDEL, T., NAGEL, G., BUCHNER, E. & FIALA, A. 2006. Light-
- 2000 induced activation of distinct modulatory neurons triggers appetitive or
- 2001 aversive learning in Drosophila larvae. *Curr Biol*, 16, 1741-7.
- 2002 SCHULTZ, W. 1998. Predictive reward signal of dopamine neurons. *J Neurophysiol*,
- 2003 80, 1-27.
- 2004 SCHURMANN, F. W. 1974. [On the functional anatomy of the corpora pedunculata in
- 2005 insects (author's transl)]. *Exp Brain Res*, 19, 406-32.
- 2006 SCHURMANN, F. W. 2016. Fine structure of synaptic sites and circuits in mushroom
- 2007 bodies of insect brains. *Arthropod Struct Dev*, 45, 399-421.
- 2008 SCHWAERZEL, M., MONASTIRIOTI, M., SCHOLZ, H., FRIGGI-GRELIN, F., BIRMAN, S. &
- 2009 HEISENBERG, M. 2003. Dopamine and octopamine differentiate between
- 2010 aversive and appetitive olfactory memories in Drosophila. *Journal of*
- 2011 *Neuroscience*, 23, 10495-10502.
- 2012 SEJOURNE, J., PLACAIS, P. Y., ASO, Y., SIWANOWICZ, I., TRANNOY, S., THOMA, V.,
- 2013 TEDJAKUMALA, S. R., RUBIN, G. M., TCHEUNIO, P., ITO, K., ISABEL, G.,
- 2014 TANIMOTO, H. & PREAT, T. 2011. Mushroom body efferent neurons
- 2015 responsible for aversive olfactory memory retrieval in Drosophila. *Nat*
- 2016 *Neurosci*, 14, 903-10.
- 2017 SHAW, S. R. & MEINERTZHAGEN, I. A. 1986. Evolutionary progression at synaptic
- 2018 connections made by identified homologous neurones. *Proc Natl Acad Sci U S*
- 2019 *A*, 83, 7961-5.
- 2020 SITARAMAN, D., ASO, Y., RUBIN, G. M. & NITABACH, M. N. 2015. Control of Sleep by
- 2021 Dopaminergic Inputs to the Drosophila Mushroom Body. *Front Neural*
- 2022 *Circuits*, 9, 73.
- 2023 STOCKER, R. F., LIENHARD, M. C., BORST, A. & FISCHBACH, K. F. 1990. Neuronal
- 2024 architecture of the antennal lobe in Drosophila melanogaster. *Cell Tissue Res*,
- 2025 262, 9-34.
- 2026 STRAUSFELD, N. J. 1976. *Atlas of an insect brain*, Berlin ; New York, Springer-Verlag.

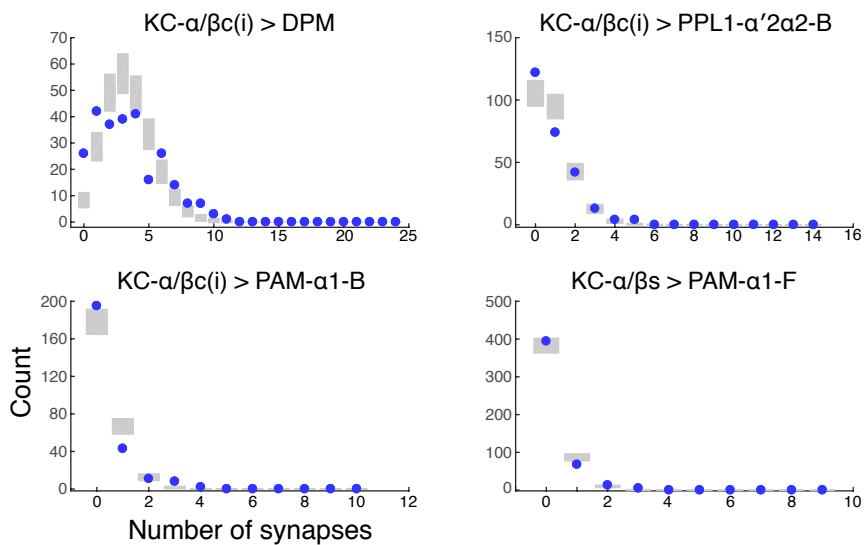
- 2027 STRAUSFELD, N. J., SINAKEVITCH, I. & VILINSKY, I. 2003. The mushroom bodies of
 2028 Drosophila melanogaster: an immunocytochemical and golgi study of Kenyon
 2029 cell organization in the calyces and lobes. *Microsc Res Tech*, 62, 151-69.
- 2030 STUBER, G. D., HNASKO, T. S., BRITT, J. P., EDWARDS, R. H. & BONCI, A. 2010.
 2031 Dopaminergic terminals in the nucleus accumbens but not the dorsal
 2032 striatum corelease glutamate. *J Neurosci*, 30, 8229-33.
- 2033 TAKEMURA, S. Y., BHARIOKE, A., LU, Z., NERN, A., VITALADEVUNI, S., RIVLIN, P. K.,
 2034 KATZ, W. T., OLBRIS, D. J., PLAZA, S. M., WINSTON, P., ZHAO, T., HORNE, J. A.,
 2035 FETTER, R. D., TAKEMURA, S., BLAZEK, K., CHANG, L. A., OGUNDEYI, O.,
 2036 SAUNDERS, M. A., SHAPIRO, V., SIGMUND, C., RUBIN, G. M., SCHEFFER, L. K.,
 2037 MEINERTZHAGEN, I. A. & CHKLOVSKII, D. B. 2013. A visual motion detection
 2038 circuit suggested by Drosophila connectomics. *Nature*, 500, 175-81.
- 2039 TAKEMURA, S. Y., LU, Z. & MEINERTZHAGEN, I. A. 2008. Synaptic circuits of the
 2040 Drosophila optic lobe: The input terminals to the medulla. *J Comp Neurol*,
 2041 509, 493-513
- 2042 TAKEMURA, S. Y., XU, C. S., LU, Z. Y., RIVLIN, P. K., PARAG, T., OLBRIS, D. J., PLAZA, S.,
 2043 ZHAO, T., KATZ, W. T., UMAYAM, L., WEAVER, C., HESS, H. F., HORNE, J. A.,
 2044 NUNEZ-IGLESIAS, J., ANICETO, R., CHANG, L. A., LAUCHIE, S., NASCA, A.,
 2045 OGUNDEYI, O., SIGMUND, C., TAKEMURA, S., TRAN, J., LANGILLE, C., LE
 2046 LACHEUR, K., MCLIN, S., SHINOMIYA, A., CHKLOVSKII, D. B.,
 2047 MEINERTZHAGEN, I. A. & SCHEFFER, L. K. 2015. Synaptic circuits and their
 2048 variations within different columns in the visual system of Drosophila.
 2049 *Proceedings of the National Academy of Sciences of the United States of*
 2050 *America*, 112, 13711-13716.
- 2051 TANAKA, N. K., AWASAKI, T., SHIMADA, T. & ITO, K. 2004. Integration of
 2052 chemosensory pathways in the Drosophila second-order olfactory centers.
 2053 *Curr Biol*, 14, 449-57.
- 2054 TANAKA, N. K., TANIMOTO, H. & ITO, K. 2008. Neuronal assemblies of the
 2055 Drosophila mushroom body. *J Comp Neurol*, 508, 711-55.
- 2056 TECHNAU, G. M. 1984. Fiber number in the mushroom bodies of adult Drosophila
 2057 melanogaster depends on age, sex and experience. *J Neurogenet*, 1, 113-26.
- 2058 TOMCHIK, S. M. & DAVIS, R. L. 2009. Dynamics of learning-related cAMP signaling
 2059 and stimulus integration in the Drosophila olfactory pathway. *Neuron*, 64,
 2060 510-21.
- 2061 TOVOTE, P., FADOK, J. P. & LUTHI, A. 2015. Neuronal circuits for fear and anxiety.
 2062 *Nat Rev Neurosci*, 16, 317-31.
- 2063 TRANNOY, S., REDT-CLOUET, C., DURA, J. M. & PREAT, T. 2011. Parallel processing
 2064 of appetitive short- and long-term memories in Drosophila. *Curr Biol*, 21,
 2065 1647-53.
- 2066 TRAUB, R. D., PAIS, I., BIBBIG, A., LEBEAU, F. E., BUHL, E. H., HORMUZDI, S. G.,
 2067 MONYER, H. & WHITTINGTON, M. A. 2003. Contrasting roles of axonal
 2068 (pyramidal cell) and dendritic (interneuron) electrical coupling in the
 2069 generation of neuronal network oscillations. *Proc Natl Acad Sci U S A*, 100,
 2070 1370-4.
- 2071 TULLY, T. & QUINN, W. G. 1985. Classical conditioning and retention in normal and
 2072 mutant Drosophila melanogaster. *J Comp Physiol A*, 157, 263-77.

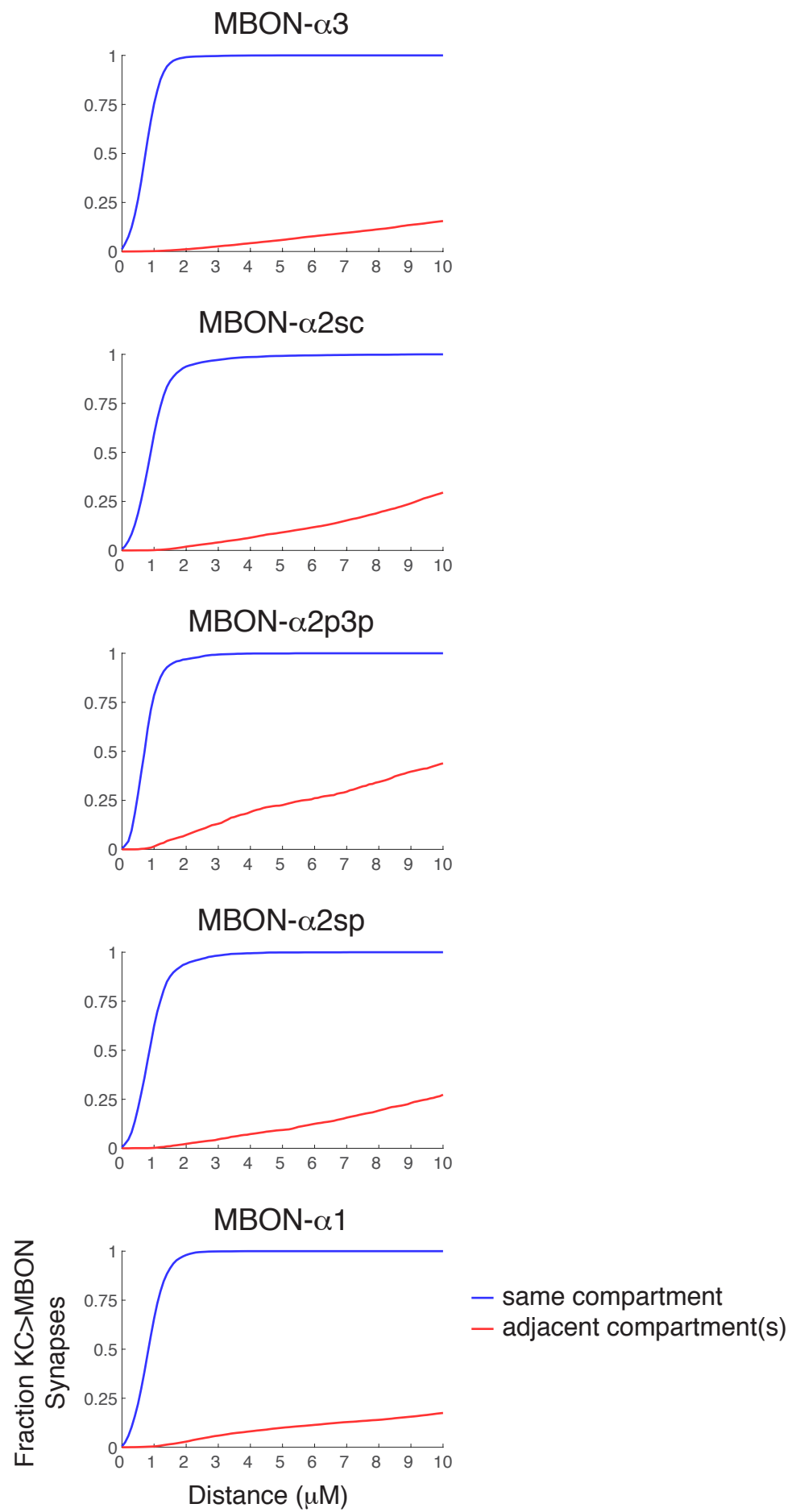
- 2073 TURNER, G. C., BAZHENOV, M. & LAURENT, G. 2008. Olfactory representations by
2074 Drosophila mushroom body neurons. *J Neurophysiol*, 99, 734-46.
- 2075 VERLEYEN, P., HUYBRECHTS, J., BAGGERMAN, G., VAN LOMMEL, A., DE LOOF, A. &
2076 SCHOOFS, L. 2004. SIFamide is a highly conserved neuropeptide: a
2077 comparative study in different insect species. *Biochem Biophys Res Commun*,
2078 320, 334-341.
- 2079 VOGT, K., ASO, Y., HIGE, T., KNAPEK, S., ICHINOSE, T., FRIEDRICH, A. B., TURNER, G.
2080 C., RUBIN, G. M. & TANIMOTO, H. 2016. Direct neural pathways convey
2081 distinct visual information to Drosophila mushroom bodies. *Elife*, 5.
- 2082 WADDELL, S. 2013. Reinforcement signalling in Drosophila; dopamine does it all
2083 after all. *Curr Opin Neurobiol*, 23, 324-9.
- 2084 WADDELL, S., ARMSTRONG, J. D., KITAMOTO, T., KAISER, K. & QUINN, W. G. 2000.
2085 The amnesiac gene product is expressed in two neurons in the Drosophila
2086 brain that are critical for memory. *Cell*, 103, 805-813.
- 2087 WONG, A. M., WANG, J. W. & AXEL, R. 2002. Spatial representation of the glomerular
2088 map in the Drosophila protocerebrum. *Cell*, 109, 229-41.
- 2089 WU, C. L., SHIH, M. F. M., LAI, J. S. Y., YANG, H. T., TURNER, G. C., CHEN, L. Y. &
2090 CHIANG, A. S. 2010. Heterotypic gap junctions between two mushroom body
2091 modulatory neurons are essential for Drosophila memory formation. *J
2092 Neurogenet*, 24, 20-21.
- 2093 WU, C. L., SHIH, M. F. M., LAI, J. S. Y., YANG, H. T., TURNER, G. C., CHEN, L. Y. &
2094 CHIANG, A. S. 2011. Heterotypic Gap Junctions between Two Neurons in the
2095 Drosophila Brain Are Critical for Memory. *Current Biology*, 21, 848-854.
- 2096 XU, C. S., HAYWORTH, K. J., LU, Z., GROB, P., HASSAN, A. M., GARCIA-CERDAN, J. G.,
2097 NIYOGI, K. K., NOGALES, E., WEINBERG, R. J. & HESS, H. F. 2017. Enhanced
2098 FIB-SEM systems for large-volume 3D imaging. *Elife*, 6.
- 2099 YAGI, R., MABUCHI, Y., MIZUNAMI, M. & TANAKA, N. K. 2016. Convergence of
2100 multimodal sensory pathways to the mushroom body calyx in Drosophila
2101 melanogaster. *Sci Rep*, 6, 29481.
- 2102 YAMAGATA, N., ICHINOSE, T., ASO, Y., PLACAIS, P. Y., FRIEDRICH, A. B., SIMA, R. J.,
2103 PREAT, T., RUBIN, G. M. & TANIMOTO, H. 2015. Distinct dopamine neurons
2104 mediate reward signals for short- and long-term memories. *Proc Natl Acad
2105 Sci U S A*, 112, 578-83.
- 2106 YI, W., ZHANG, Y., TIAN, Y., GUO, J., LI, Y. & GUO, A. 2013. A subset of cholinergic
2107 mushroom body neurons requires go signaling to regulate sleep in
2108 Drosophila. *Sleep*, 36, 1809-21.
- 2109 YU, D., AKALAL, D. B. & DAVIS, R. L. 2006. Drosophila alpha/beta mushroom body
2110 neurons form a branch-specific, long-term cellular memory trace after
2111 spaced olfactory conditioning. *Neuron*, 52, 845-55.
- 2112 YU, D., KEENE, A. C., SRIVATSAN, A., WADDELL, S. & DAVIS, R. L. 2005a. Drosophila
2113 DPM neurons form a delayed and branch-specific memory trace after
2114 olfactory classical conditioning. *Cell*, 123, 945-57.
- 2115 YU, D. H., KEENE, A. C., SRIVATSAN, A., WADDELL, S. & DAVIS, R. L. 2005b.
2116 Drosophila DPM neurons form a delayed and branch-specific memory trace
2117 after olfactory classical conditioning. *Cell*, 123, 945-957.

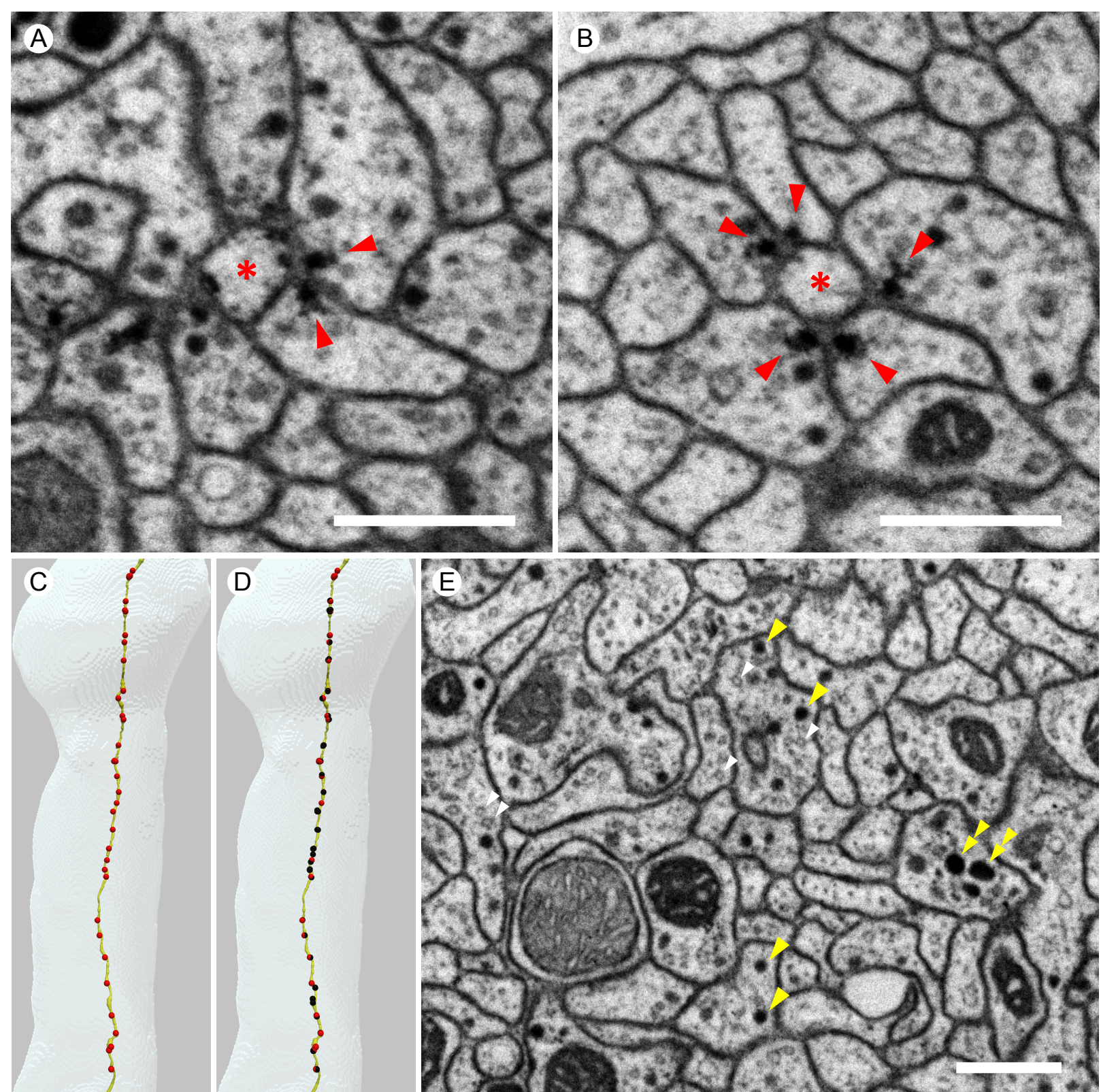
- 2118 ZARS, T., FISCHER, M., SCHULZ, R. & HEISENBERG, M. 2000. Localization of a short-
2119 term memory in Drosophila. *Science*, 288, 672-5.
- 2120 ZHANG, J., BERRIDGE, K. C., TINDELL, A. J., SMITH, K. S. & ALDRIDGE, J. W. 2009. A
2121 neural computational model of incentive salience. *PLoS Comput Biol*, 5,
2122 e1000437.
- 2123 ZHAO, T., OLBRIS, D. J., YU, Y. & PLAZA, S. 2017. NeuTu-EM. Github.
2124 d792abd3981b1bf77c87368cf8df6e48c54acb87.
2125 https://github.com/janelia-flyem/NeuTu/tree/flyem_release
- 2126 ZHOU, F. W., JIN, Y., MATTA, S. G., XU, M. & ZHOU, F. M. 2009. An ultra-short
2127 dopamine pathway regulates basal ganglia output. *J Neurosci*, 29, 10424-35.
- 2128

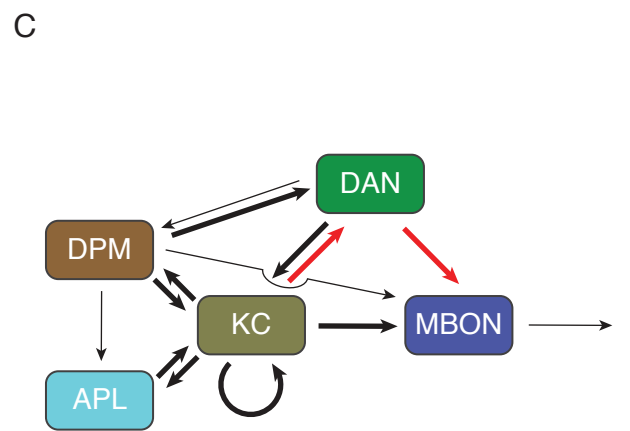
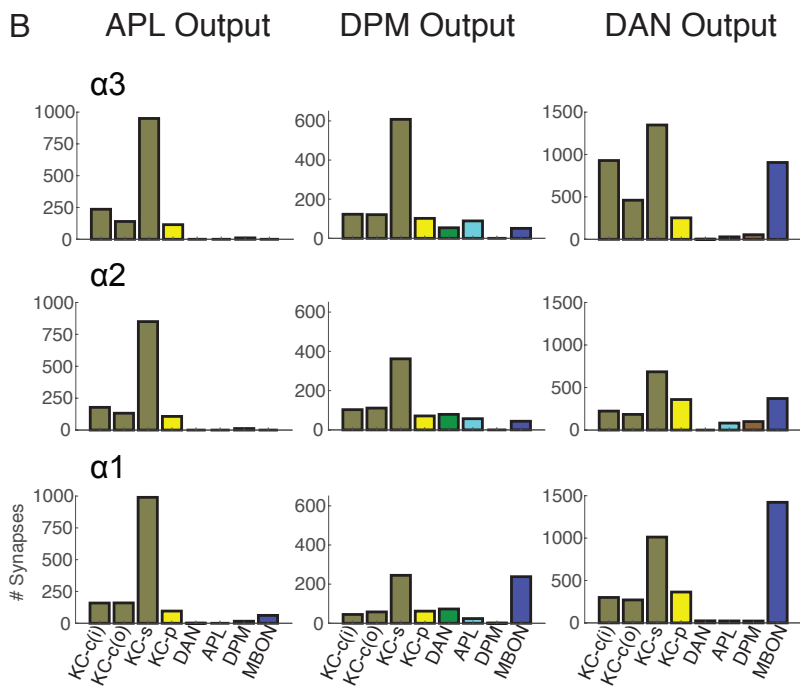
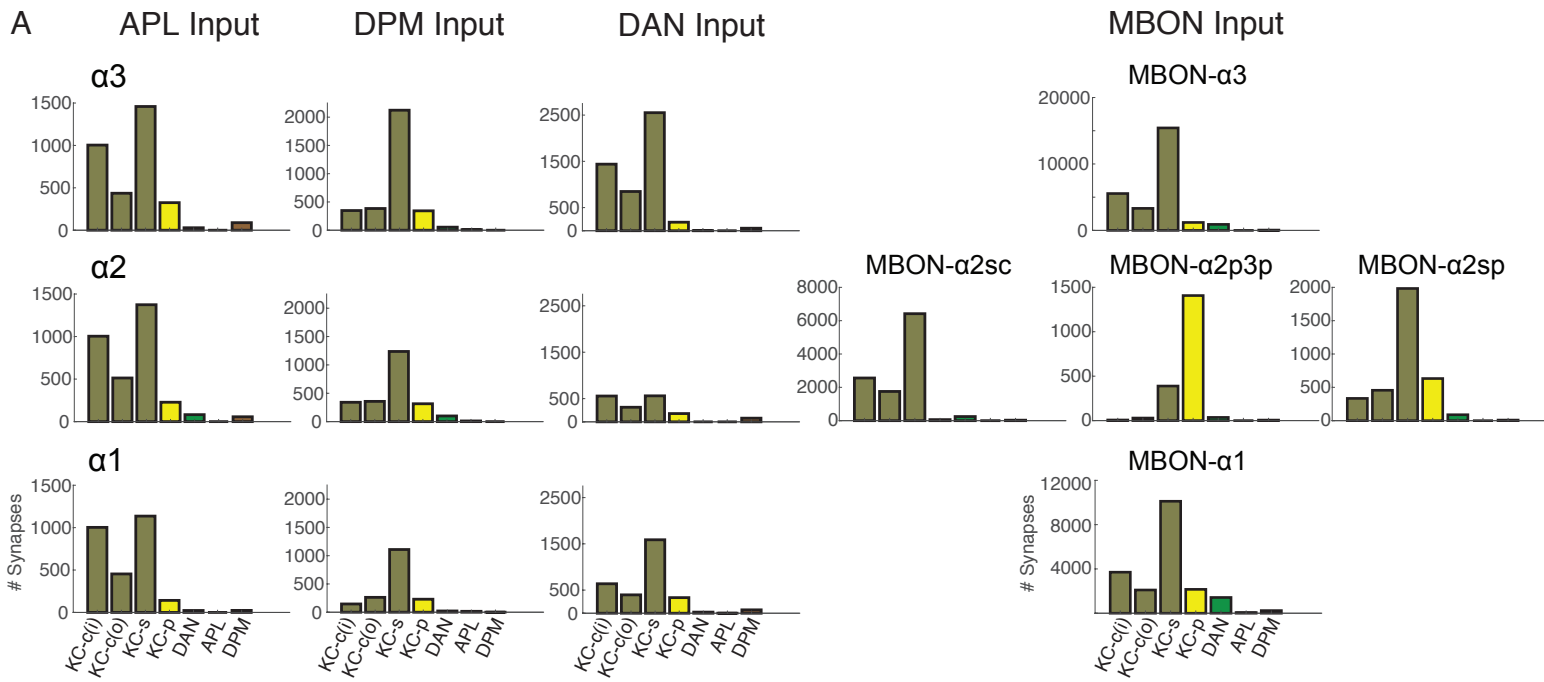
A**B**

Pre	KC $\alpha/\beta c(i)$	KC $\alpha/\beta c(o)$	KC $\alpha/\beta s$	KC $\alpha/\beta p$
MBON- $\alpha 3\text{-}A$	0.380	0.995	0.140	0.945
MBON- $\alpha 3\text{-}B$	0.793	0.113	0.220	0.881
MBON- $\alpha 2sc$	0.000	0.380	0.827	0.153
MBON- $\alpha 2p3p\text{-}A$	0.743	0.845	0.000	0.828
MBON- $\alpha 2p3p\text{-}B$	1.000	0.915	0.000	0.760
MBON- $\alpha 2sp$	0.000	0.957	0.003	0.671
MBON- $\alpha 1\text{-}A$	0.235	0.769	0.423	0.488
MBON- $\alpha 1\text{-}B$	0.019	0.604	0.046	0.290
PPL1- $\alpha 3\text{-}A$	0.909	0.822	0.483	0.719
PPL1- $\alpha 3\text{-}B$	0.543	0.797	0.041	0.216
PPL1- $\alpha'2a2\text{-}A$	0.003	0.001	0.170	0.901
PPL1- $\alpha'2a2\text{-}B$	0.000	0.917	0.001	0.869
PAM- $\alpha 1\text{-}A$	0.858	0.430	0.813	0.780
PAM- $\alpha 1\text{-}B$	0.000	0.629	0.004	0.996
PAM- $\alpha 1\text{-}C$	0.002	0.719	0.152	0.553
PAM- $\alpha 1\text{-}D$	0.113	0.189	0.004	0.743
PAM- $\alpha 1\text{-}E$	0.046	0.528	0.005	0.982
PAM- $\alpha 1\text{-}F$	0.012	0.685	0.000	0.982
PAM- $\alpha 1\text{-}G$	0.451	0.842	0.166	0.028
PAM- $\alpha 1\text{-}H$	0.774	0.985	0.819	0.982
PAM- $\alpha 1\text{-}I$	1.000	0.996	0.062	0.320
PAM- $\alpha 1\text{-}J$	0.953	0.072	0.015	1.000
PAM- $\alpha 1\text{-}K$	0.997	0.950	0.459	0.865
PAM- $\alpha 1\text{-}L$	0.476	0.327	0.204	0.567
PAM- $\alpha 1\text{-}M$	0.359	0.755	0.928	0.879
PAM- $\alpha 1\text{-}N$	1.000	1.000	0.264	0.893
PAM- $\alpha 1\text{-}O$	1.000	0.999	0.011	0.940
PAM- $\alpha 1\text{-}P$	1.000	1.000	0.554	0.925
APL	0.424	0.484	0.771	0.771
DPM	0.000	0.948	0.200	0.110

C

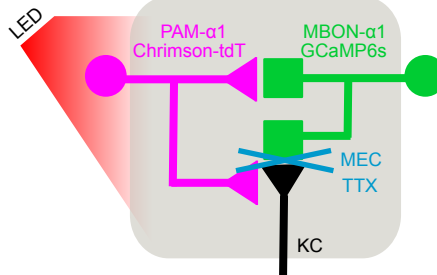
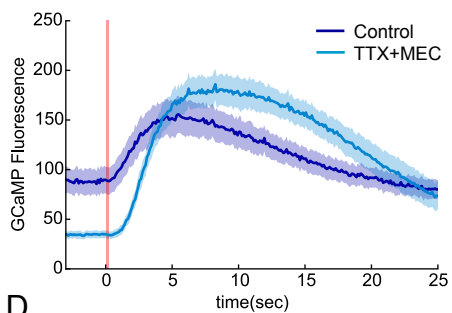
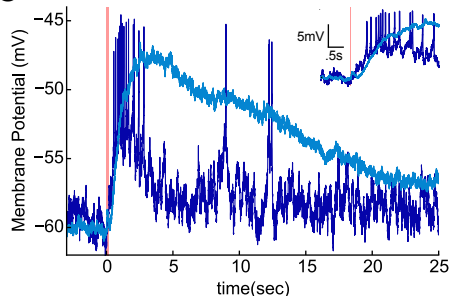
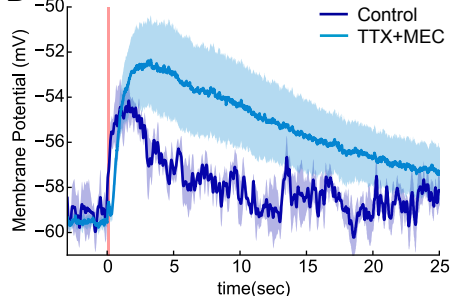
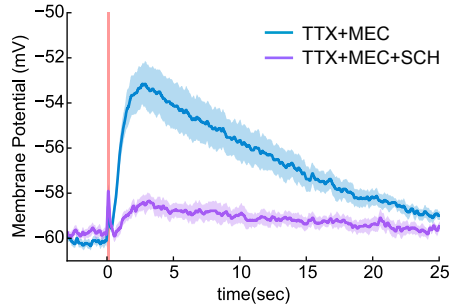
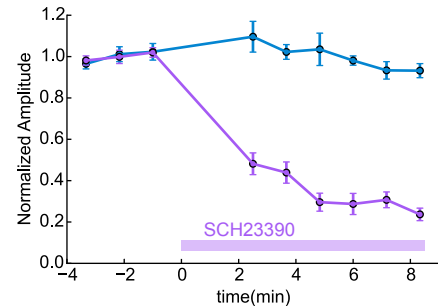


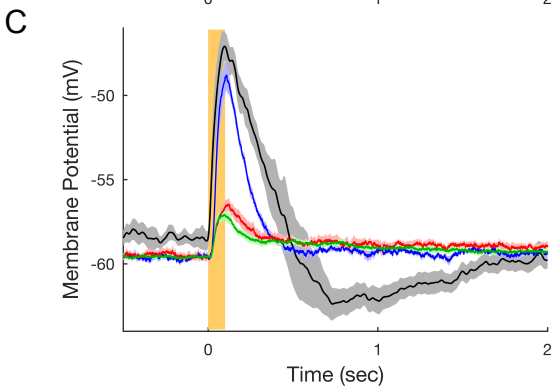
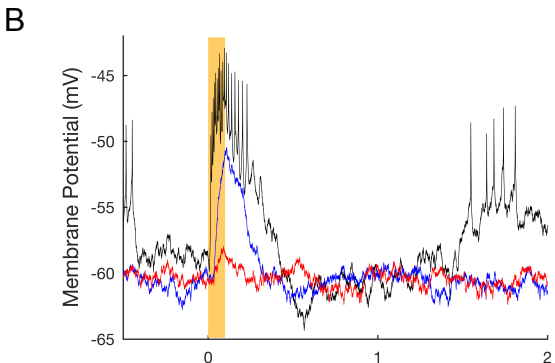
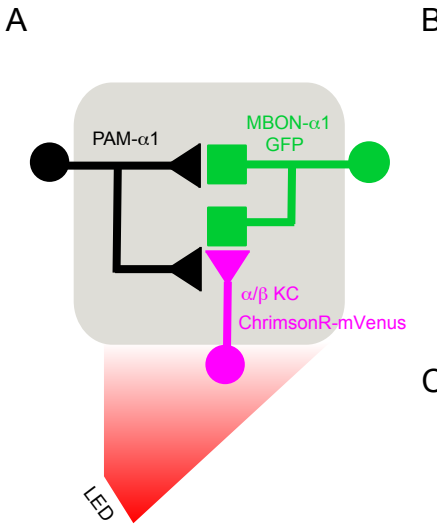




	To From	KC $\alpha/\beta c(i)$	KC $\alpha/\beta c(o)$	KC $\alpha/\beta s$	KC $\alpha/\beta p$	PPL	PAM	MBON- α_3	MBON- α_{2sc}	MBON- α_{2p3p}	MBON- α_{2sp}	MBON- α_1	APL	DPM
α_3	KC $\alpha/\beta c(i)$	6786	1220	367	0	1439	0	5549	63	0	0	0	1004	348
α_2	KC $\alpha/\beta c(i)$	4169	510	72	0	556	15	308	2560	334	7	162	1004	341
α_1	KC $\alpha/\beta c(i)$	7039	774	126	0	2	637	0	4	0	0	3706	1003	146
α_3	KC $\alpha/\beta c(o)$	1108	1991	1338	0	848	0	3317	52	0	0	0	436	384
α_2	KC $\alpha/\beta c(o)$	532	1472	652	0	314	23	72	1753	456	29	88	513	357
α_1	KC $\alpha/\beta c(o)$	783	1812	1055	0	0	397	0	0	9	0	2098	454	263
α_3	KC $\alpha/\beta s$	365	1428	19922	373	2552	0	15425	362	40	13	0	1459	2123
α_2	KC $\alpha/\beta s$	75	717	9401	220	560	46	31	6419	1983	389	250	1374	1237
α_1	KC $\alpha/\beta s$	134	1099	13346	413	1	1588	0	0	12	0	10111	1136	1109
α_3	KC $\alpha/\beta p$	0	0	293	1806	184	0	1196	5	59	158	0	325	343
α_2	KC $\alpha/\beta p$	0	0	137	1378	178	0	0	62	632	1407	0	228	315
α_1	KC $\alpha/\beta p$	0	2	338	2378	3	337	0	0	2	0	2155	142	230
α_3	PPL	929	461	1348	253	2	0	906	2	1	2	0	29	54
α_2	PPL	223	184	685	359	0	0	2	246	89	36	0	82	100
α_1	PPL	0	0	1	4	0	0	0	0	1	0	0	0	0
α_3	PAM	0	0	0	0	0	0	0	0	0	0	0	0	0
α_2	PAM	9	9	31	0	0	0	0	0	0	0	22	0	0
α_1	PAM	300	271	1012	364	0	24	0	0	0	0	1422	23	22
α_3	APL	236	140	950	115	0	0	0	0	0	0	0	0	11
α_2	APL	178	132	850	107	0	0	0	0	0	0	1	0	12
α_1	APL	159	160	990	96	0	1	0	0	0	0	62	0	16
α_3	DPM	123	121	608	102	54	0	51	2	0	1	0	89	0
α_2	DPM	103	111	362	71	79	7	0	29	9	6	7	57	0
α_1	DPM	45	58	245	62	0	73	0	0	0	0	238	24	1

Figure 6 – figure supplement 1

A**B****C****D****E****F**



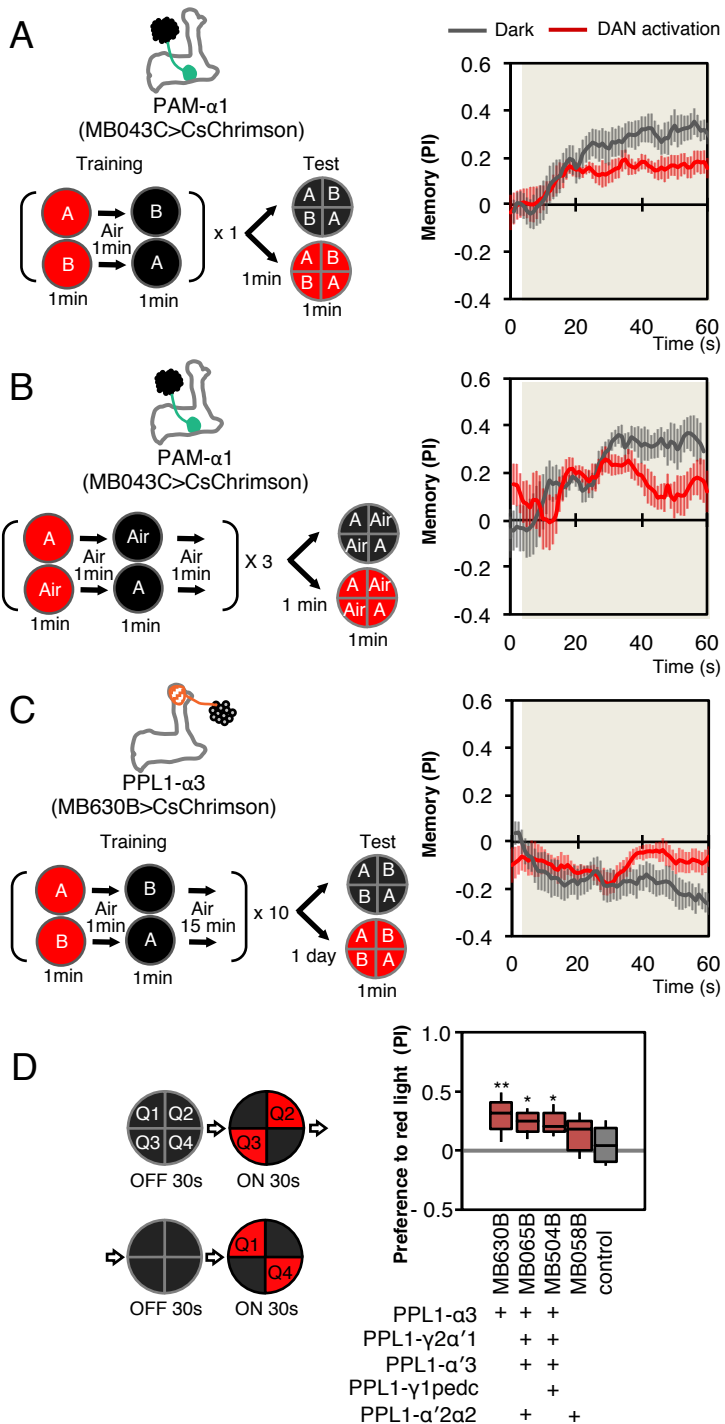


Figure 8

